atmosphere

MDPI

Article

Quantification of Multi-Source Road Emissions in an Urban Environment Using Inverse Methods

Panagiotis Gkirmpas [1,2,*], George Tsegas [1], Giannis Ioannidis [3], Paul Tremper [4], Till Riedel [4], Eleftherios Chourdakis [1], Christos Vlachokostas [1] and Nicolas Moussiopoulos [5]

[1] Sustainability Engineering Laboratory, Aristotle University of Thessaloniki, 54124 Thessaloniki, Greece
[2] Laboratory of Atmospheric Physics, School of Physics, Aristotle University of Thessaloniki, 54124 Thessaloniki, Greece
[3] Climate and Atmosphere Research Centre, The Cyprus Institute, 2121 Nicosia, Cyprus
[4] TECO/Pervasive Computing Systems, Karlsruhe Institute of Technology (KIT), 76131 Karlsruhe, Germany
[5] Main Campus, Aristotle University of Thessaloniki, 54124 Thessaloniki, Greece
* Correspondence: pgkirmpas@auth.gr

Abstract

The spatial quantification of multiple sources within the urban environment is crucial for understanding urban air quality and implementing measures to mitigate air pollution levels. At the same time, emissions from road traffic contribute significantly to these concentrations. However, uncertainties arise when assessing the contribution of multiple sources affecting a single receptor. This study aims to evaluate an inverse dispersion modelling methodology that combines Computational Fluid Dynamics (CFD) simulations with the Metropolis–Hastings Markov Chain Monte Carlo (MCMC) algorithm to quantify multiple traffic emissions at the street scale. This approach relies solely on observational data and prior information on each source's emission rate range and is tested within the Augsburg city centre. To address the absence of extensive measurement data of a real pollutant correlated with traffic emissions, a synthetic observational dataset of a theoretical pollutant, treated as a passive scalar, was generated from the forward dispersion model, with added Gaussian noise. Furthermore, a sensitivity analysis also explores the influence of sensor configuration and prior information on the accuracy of the emission estimates. The results indicate that, when the potential emission rate range is narrow, high-quality predictions can be achieved (ratio between true and estimated release rates, $\Delta q \leq 2$) even with networks using data from only 10 sensors. In contrast, expanding the allowable emission range leads to reduced accuracy ($2 \leq \Delta q \leq 6$), particularly in networks with fewer than 50 sensors. Further research is recommended to assess the methodology's performance using real-world measurements.

Keywords: inverse dispersion modelling; traffic emissions; multiple source quantification; sensor configuration analysis; computational fluid dynamics; Bayesian inference; urban environment

Academic Editor: Andrea Spinazzè

Received: 20 August 2025
Revised: 6 October 2025
Accepted: 11 October 2025
Published: 14 October 2025

Citation: Gkirmpas, P.; Tsegas, G.; Ioannidis, G.; Tremper, P.; Riedel, T.; Chourdakis, E.; Vlachokostas, C.; Moussiopoulos, N. Quantification of Multi-Source Road Emissions in an Urban Environment Using Inverse Methods. *Atmosphere* **2025**, *16*, 1184. https://doi.org/10.3390/atmos16101184

1. Introduction

Air pollution can cause serious health risks and negative impacts on populations since it is one of the major environmental stressors [1,2]. According to the World Health Organization (WHO), exposure to air pollutants is one of the major environmental risks to child health. The WHO estimates that in 2019 outdoor air pollution caused 4.2 million

premature deaths worldwide [3]. The same organization links exposure to airborne contaminants with several negative impacts on human health, which can lead to diseases, such as ischemic heart disease, stroke, chronic obstructive pulmonary disease, acute lower respiratory infections, and lung cancer [3].

Recognition and quantification of emissions from multiple sources are of great importance, as they provide information about each source's contribution to Air Quality (AQ) levels. Such information is crucial for relevant authorities and policy makers to adopt measures aimed at reducing air pollution and controlling AQ. At the same time, the estimation of emissions from multiple sources is essential for emission inventory purposes. The quality of emission inventories is one of the most important factors that strongly affect the accuracy and results of Atmospheric Transport and Dispersion (ATD) models.

The field of inverse dispersion modelling has been extensively studied in previous research, primarily to identify one or a few unknown sources and estimate their release rates. This process, known as Source Term Estimation (STE), has a wide range of applications documented in the literature [4]. STE methods have been applied at various spatial scales, from global [5] and regional [6,7] to urban [8] and street scale [9]. In parallel, several studies have evaluated STE techniques using real-world applications [10,11] and datasets, as well as using data from field [12–15] and wind tunnel experiments [16–18]. Additionally, in many cases, synthetic observational datasets have been generated and used to test inverse dispersion modelling techniques, addressing the lack of real measurements [11,19–21].

In urban environments, where complex structures significantly influence pollutant dispersion due to strong turbulence caused by the interaction between wind flow and urban geometry, Computational Fluid Dynamics (CFD) models are capable of providing accurate street-scale pollutant concentration predictions. CFD has been employed in numerous studies involving both forward [22–24] and inverse dispersion modelling [10,11,25].

An inverse dispersion modelling methodology involves the calculation of the source–receptor relationship, which describes the sensitivity of receptor measurements to emissions from potential source locations. The source receptor relationship can be calculated either by applying the ATD model in terms of "forward" simulations by solving the advection-diffusion equation for each source or by applying the ATD model in terms of "backward" simulations by solving the adjoint advection-diffusion equation for every sensor as source. The present work uses the "forward" mode of inverse modelling and solves the ATD model for every road traffic source once.

To estimate the unknown parameters of air pollution sources, different types of methods and algorithms have been applied using datasets derived from both measured and modelled concentrations. Most of the previous inverse dispersion modelling studies have used optimization [12,26,27], probabilistic [10,25,28,29], or recently machine learning algorithms [30,31]. In this work, the Metropolis–Hastings Markov Chain Monte Carlo (MCMC) algorithm, which is based on Bayesian inference, is applied to estimate the emission rate of each one of the multiple sources. In the following subsections are presented the source–receptor relationship, the Bayesian inference and the Metropolis–Hastings MCMC as they used in the present study.

Quantification of air pollution sources has been widely investigated within the broader research field of source apportionment. According to Coelho et al. [32] source apportionment methods provide essential insights into the relative contributions of different emission categories (e.g., transportation, residential heating, industrial activities) and emission areas (e.g., local, urban, metropolitan, or regional scales) to ambient pollutant concentrations. These techniques are primarily applied to quantify emissions from specific source sectors or areas, rather than from individual sources within the same sector in the same region. On the other hand, inverse dispersion algorithms, when combined with atmospheric transport

and dispersion (ATD) models, can quantify the contributions of individual sources within a specific sector. Feng et al. [33] employed Bayesian inference together with the WRF-CMAQ chemical transport model to update the SO_2 emission inventory for Chongqing, China. Although that work focused on emissions at the urban scale, the WRF-CMAQ application was conducted on a 5×5 km^2 domain. Similarly, Cheng et al. [34] introduced an inverse modelling methodology based on DDM-3D and 3DVAR techniques, coupled with WRF-CMAQ simulations, to estimate SO_2, NO_2, and O_3 emissions in the Beijing–Tianjin–Hebei region, China at $1^\circ \times 1^\circ$ resolution. Kumar et al. [35] applied an inverted Fixed Box Model (FBM) to estimate emissions from regulated air pollutants in the Delhi, India.

In the road traffic sector, emissions from multiple roads can be quantified using integrated tools such as COPERT [36]. These tools provide detailed estimates based on traffic activity, vehicle fleet composition, speed, and other factors. However, while multiple-source quantification is feasible, relatively few studies have explored this approach. For instance, Carruthers et al. [37] combined an inverse modelling technique with the Gaussian plume dispersion model ADMS-Urban to improve the traffic emission inventory in Cambridge, UK.

The studies mentioned above, which address multiple-source emission estimation, either use very coarse spatial resolution [33,34] or rely on simplified models [35,37]. From this perspective, no prior research in the literature has demonstrated the ability to predict emissions at street scale. This study addresses that gap by presenting a novel methodology for estimating emission rates from multiple traffic-related road sources at very high resolution. For this purpose, the OpenFOAM CFD model was combined with the Metropolis–Hastings MCMC algorithm to calculate the emission rates of 69 traffic-related road sources in the city centre of Augsburg, Germany. To address the absence of real measurements of a regulated air pollutant, synthetic observations of a theoretical pollutant were generated using the forward model concentrations with added Gaussian noise. The algorithm is applied under various sensor configurations, wind directions, and levels of prior information to evaluate the influence of sensor quantity and prior knowledge on the accuracy of estimated release rates.

2. Materials and Methods

2.1. Methodology

The methodology of the current study involves the following computational steps:

- Airflow simulation is applied to calculate wind flow and turbulence parameters under steady-state conditions for the wind directions of interest. A total of 36 wind direction sectors is considered, ranging from 0° to 350° in 10-degree increments.
- The source–receptor relationships are calculated using a forward dispersion model for each individual road traffic emission source.
- A synthetic observational dataset of a theoretical pollutant is generated by adding Gaussian noise to the concentrations obtained from the forward dispersion model.
- The Metropolis–Hastings MCMC algorithm is employed to estimate the release rate of each traffic source, based on both modelled and synthetic measured concentrations, incorporating prior knowledge of the emission rate range for each source.
- The Metropolis–Hastings MCMC is applied across various sensor configurations, involving different numbers of sensors and wind directions. Specific prior knowledge is used for all algorithm runs to assess the impact of sensor quantity on the accuracy of release rate estimations.
- The previous step is repeated using different emission rate ranges as prior information to examine how variations in prior knowledge influence the resulting release rate estimates.

For clarity, Figure 1 provides a visual illustration of the computational steps in the proposed methodology.

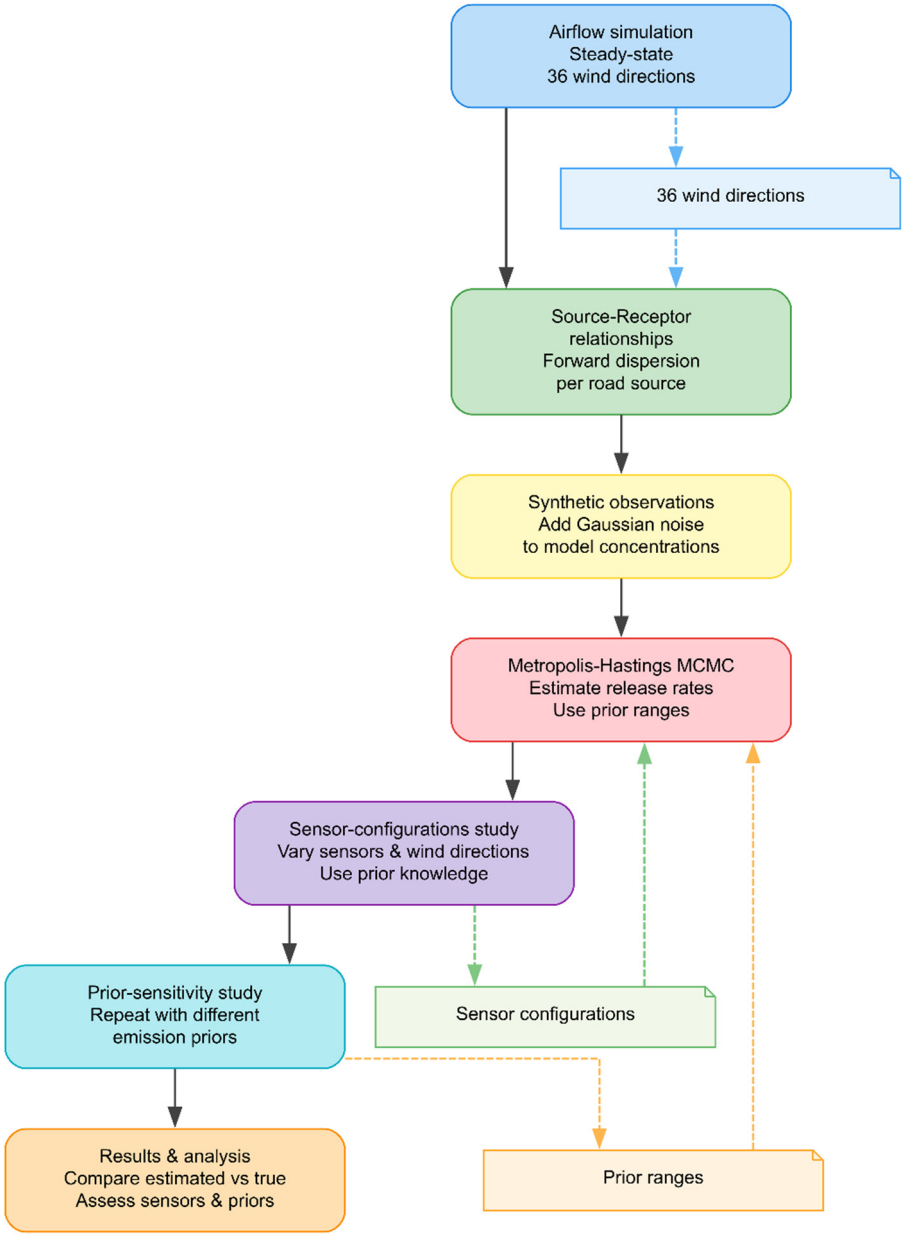

Figure 1. Flowchart of the computational steps in the methodology.

2.2. Source–Receptor Relationship

To simulate the transport and dispersion of an airborne pollutant within a specific area, various ATD models can be applied. In CFD modelling, the advection–diffusion equation is widely used due to its ability to accurately predict pollutant concentration fields in three-dimensional discretized space.

Assume a line source $r(l) = (x(l), y(l), z(l))$, positioned in Cartesian space (x, y, z) and continuously emitting a passive pollutant, treated as a scalar, at a rate q_s. Here, l is a parametric variable representing the length along the road. The transport of the scalar in the spatial domain is governed by the advection–diffusion equation:

$$\frac{\partial C}{\partial t} + u_j \frac{\partial C}{\partial x_j} - \frac{\partial}{\partial x_j} D \frac{\partial C}{\partial x_j} = q_s \delta(r(l)) \quad (1)$$

where

- C is the concentration of the passive scalar;
- $u_j = (u, v, w)$ represents the velocity vector in Cartesian coordinates $x_j = (x, y, z)$;
- D is the diffusion coefficient;
- $\delta(\cdot)$ is the Dirac delta function, representing the source.

$$D = D_m + D_t = D_m + \frac{v_t}{Sc_t} \tag{2}$$

Here

- Sc_t is the turbulent Schmidt number;
- v_t is the eddy viscosity.

Substituting Equation (2) into Equation (1), the advection–diffusion equation becomes:

$$\frac{\partial C}{\partial t} + u_j \frac{\partial C}{\partial x_j} - \frac{\partial}{\partial x_j}\left(D_m + \frac{v_t}{Sc_t}\right)\frac{\partial C}{\partial x_j} = q_s \delta(r(l)) \tag{3}$$

The source–receptor relationship quantifies the sensitivity of concentration observed at each sensor in a monitoring network, based on a specific set of source parameters, $s = (r(l), q_s)$. Using a forward dispersion model, the source–receptor relationship ${C^c}_i$ for each sensor i, located at (x_n, y_n, z_n), is defined by the concentration of the passive scalar, C, as follows:

$$C^c(s)_i = C(x_n, y_n, z_n)_i \tag{4}$$

2.3. Bayesian Inference

Bayesian inference is a probabilistic framework that combines prior knowledge with both observed and simulated data to draw conclusions. It has been widely applied in conjunction with Computational Fluid Dynamics (CFD) simulations to estimate unknown source parameters [10,25,38,39]. These Bayesian methods, grounded in Bayes' theorem, calculate the posterior probability of source parameters by integrating the following:

- Existing knowledge about the source term;
- Uncertainties in sensor data;
- Possible inaccuracies in model predictions.

Let d represent the air pollutant concentration observations from a sensor network, and s denote the source characteristics (including the release rate). According to the Bayes' theorem, the posterior probability distribution $p(s|d)$ describes the probability of the source term s given the measurements d and is calculated as follows:

$$p(s|d) = \frac{p(d|s)p(s)}{p(d)} \propto p(d|s)p(s) \tag{5}$$

where

- $p(d|s)$ is the likelihood, indicating the probability of observing d given source s;
- $p(s)$ is the prior distribution, representing known information about s before the analysis;
- $p(d)$ is the evidence or normalization factor, which is independent of s and ensures the posterior is a valid probability distribution.

2.3.1. Likelihood Function

In inverse dispersion modelling, the likelihood function expresses the probability of observing a given set of sensor measurements d_i assuming a specific source term s.

Practically, it measures the discrepancy between the model-predicted concentrations $C_i(s)$ and the actual measured concentrations d_i at sensor location i. The vector of the estimated parameters can be defined as $s = (x_s, q_s)$, where x_s represents of the source location, and q_s denotes the release rate.

The following vectors are defined:

- $C^{true} \in \mathbb{R}^N$: the (unknown) true concentrations at the sensor locations;
- $d \in \mathbb{R}^N$: the observed concentrations from the sensor network;
- $C^c(s) \in \mathbb{R}^N$: the concentrations computed by the ATDM based on source term s;
- N: the overall number of sensors.

The observations and model predictions are linked to the true concentrations via the following error terms:

$$d = C^{true} + \varepsilon^o \tag{6}$$

$$C^c(s) = C^{true} + \varepsilon^c \tag{7}$$

Here

- ε^o is the measurement error vector;
- ε^c is the model error vector.

Estimating these error components is particularly challenging [40]. According to Yee et al. [10], the model error is generally the dominant source of uncertainty and is difficult to characterize due to its complex origins. Consequently, a common assumption in the literature is that both ε^o and ε^c follow a specific distribution. Although Wang et al. [41] compared various assumptions about the error distribution and found no clear superiority among them, in the inverse dispersion modelling literature [25,38,39,42], the simplest and widely used assumption is that the errors ε^o and ε^c follow a Gaussian distribution with a mean of zero and variances σ_o^2 and σ_c^2, respectively. Under these assumptions, the probabilities associated with the measurement and model errors are as follows:

$$p\left(d\middle|C^{true}\right) \propto exp\left[-\frac{1}{2}\sum \frac{\left(d_i - {C^{true}}_i\right)^2}{\sigma_{o,i}^2}\right] \tag{8}$$

$$p\left(C^{true}\middle|s\right) \propto exp\left[-\frac{1}{2}\sum \frac{\left({C^{true}}_i - C^c(s)_i\right)^2}{\sigma_{c,i}^2}\right] \tag{9}$$

where $i \in [1, N]$ is the index of each sensor. Using, the $p\left(d\middle|C^{true}\right)$ and $p\left(C^{true}\middle|s\right)$ probabilities the likelihood function becomes:

$$p(d|s) \propto \int_{C^{true}} p\left(d\middle|C^{true}\right) p\left(C^{true}\middle|s\right) dC^{true} \propto exp\left[-\frac{1}{2}\sum \frac{\left({C^o}_i - C^c(s)_i\right)^2}{\sigma_{o,i}^2 + \sigma_{c,i}^2}\right] \tag{10}$$

2.3.2. Prior Probability

The prior probability incorporates any existing knowledge about the source characteristics before performing inference. Prior information can improve both the speed and accuracy of the inference process [42]. In the current study, the release rate is assumed to take any value within a predefined range and must always remain positive. Under this assumption, the prior probability is defined as follows:

$$p(s) = \begin{cases} \text{constant, } if\ q_s > 0 \text{ and } q_{s_{min}} < q_s < q_{s_{max}} \\ 0, \text{ else} \end{cases} \tag{11}$$

Here, $q_{s_{min}}$ and $q_{s_{max}}$ represent the predefined minimum and maximum release rates, respectively, specified prior to the inference process.

2.3.3. Posterior Probability

The posterior probability is derived by combining the likelihood function (Equation (10)) and the prior distribution (Equation (11)) in Equation (5) as follows:

$$p(s|d) \propto \begin{cases} exp\left[-\frac{1}{2}\sum \frac{(C^o{}_i - C^c(\theta)_i)^2}{\sigma^2_{o,i}+\sigma^2_{c,i}}\right], \text{if } q_s > 0 \text{ and } q_{s_{min}} < q_s < q_{s_{max}} \\ 0, \text{ else} \end{cases} \quad (12)$$

2.3.4. Sampling Methods

The posterior probability can be evaluated for every possible release rate of each source within the predefined prior range. However, this approach can significantly increase the computational resources required to compute the posterior probabilities and identify their maximum, potentially making the process impractical. To address this, sampling methods are employed to generate representative samples and provide the final estimated release rates in the form of probability density functions (PDFs).

There are different categories of sampling techniques, such as Markov Chain Monte Carlo (MCMC) methods [43], Importance Sampling [44], Rejection Sampling [45], and Sequential Monte Carlo [46]. Among them, the most widely used in source parameter estimation is the MCMC method. Various MCMC algorithms have been used in previous studies, but the most popular among them is the Metropolis–Hastings MCMC algorithm.

2.3.5. Metropolis–Hastings MCMC

MCMC algorithms generate a Markov chain of samples whose stationary distribution is proportional to the target PDF (posterior distribution). Although MCMC tends to sample more frequently from high-probability regions, it can still generate samples from low-probability regions, particularly due to the stochastic nature of the process and the proposal mechanism used in some MCMC algorithms, such as the widely used Metropolis–Hastings algorithm [25]. A detailed description of the Metropolis–Hastings algorithm can be found in [43,47]. The computational steps of the algorithm are as follows:

- Initialize: set the initial state x^0.
- For $i = 0, 1, 2, \ldots, N$:
    - Sample the proposal state $x' \sim q(x'/x)$.
    - Calculate the acceptance probability $a = \frac{p(x')q(x/x')}{p(x)q(x'/x)}$.
    - A random number uniformly sampled between 0 and 1: $u \sim U(0,1)$.
    - If $u < a$:
        - Accept the proposal state $x^{i+1} = x'$.
    - Else:
        - Reject the proposal state $x^{i+1} = x^i$.
- Store the sample x.

Here, N is the total number of iterations, $p(x)$ is the target distribution and $q(x'/x)$ is the proposal distribution from which the candidate samples are drawn. In cases where a symmetric distribution (e.g., Gaussian) is assumed, the acceptance probability is simplified to $a = \frac{p(x')}{p(x)}$. Therefore, in cases where the sample x' has a higher posterior probability $p(x')$, than x $(p(x))$, the acceptance probability a exceeds 1, and x' is accepted. However, even when $p(x')$ is lower than $p(x)$, x' may still be accepted if $u < a$. This criterion prevents the algorithm from getting trapped in local optima.

2.4. Case Study

For this study, the city centre of Augsburg, Germany, was selected as the case study area due to its representative geometrical and topological features typical of Central European cities. The actual city layout is presented in Figure 2a, while Figure 2b shows the simplified geometry model used in the simulations. The 3D urban model was developed using data from OpenStreetMap (OSM) [48], an open-source, community-driven platform for collecting and sharing geographic information. OSM provides detailed 2D building footprints and height data, and prior research [49–51] has demonstrated its reliability and accuracy, often matching commercial data sources, particularly in urban settings.

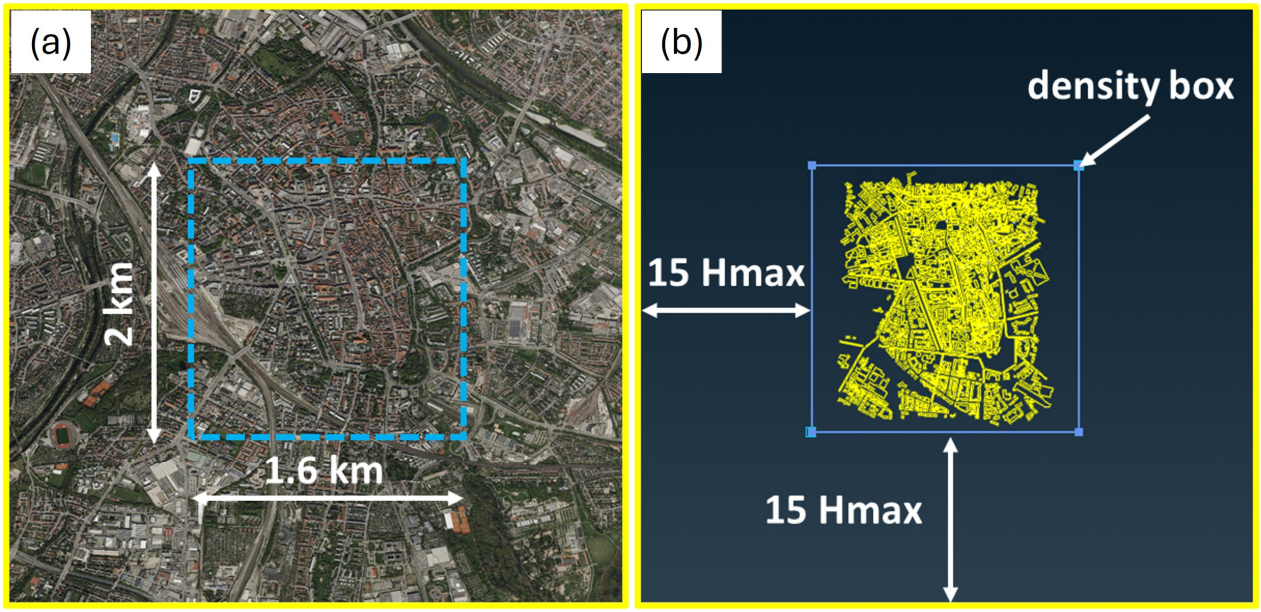

Figure 2. Area of interest in Augsburg (**a**) and computational domain containing the city's digital model (**b**).

In this study, buildings were modelled with flat rooftops, and ventilation structures were neglected. These simplifications, commonly applied in urban dispersion modelling [52], are not expected to significantly impact simulation accuracy. A pre-processing step was applied to the urban geometry to correct surface inconsistencies, ensuring that the data could be directly used for generating the computational mesh without further adjustments. Accurate representation of the urban structure is essential for CFD-based air quality modelling [53]. Figure 2a outlines the 2×1.6 km^2 study domain, where the maximum building height (H_{max}) is 83.5 m. As shown in Figure 2b, the computational domain extends beyond the immediate area of interest, with an upstream distance of $15H_{max}$, and a vertical extent of $6H_{max}$ [54].

The commercial pre-processor tool ANSA [55] was used to construct the computational mesh, which incorporates the city's geometrical characteristics. The resolution for the buildings was set at 1 m, allowing for high spatial accuracy of the CFD outputs, with increased refinement in the areas of street canyons. For the high refinement demands of the traffic emission sources (used in the multiple traffic emission source quantification application), the resolution was set at 0.25 m. The resolution at the boundaries of the domain was set at 30 m.

The characteristics of the computational mesh are presented in Figure 3. Specifically, Figure 3a shows the mesh elements and the higher-density region in the urban area in the $x - y$ plane, while Figure 3b illustrates the structure of the computational cells on the

ground, building surfaces, and traffic sources. The total number of computational cells is 48,046,100, and the mesh consists of unstructured tetrahedral cells. The dimensionless parameter y^+, which indicates mesh quality near wall surfaces, was calculated to be 255 for the ground and 151 for the buildings, meaning that both values fall within the acceptable range of 30 to 300 [56].

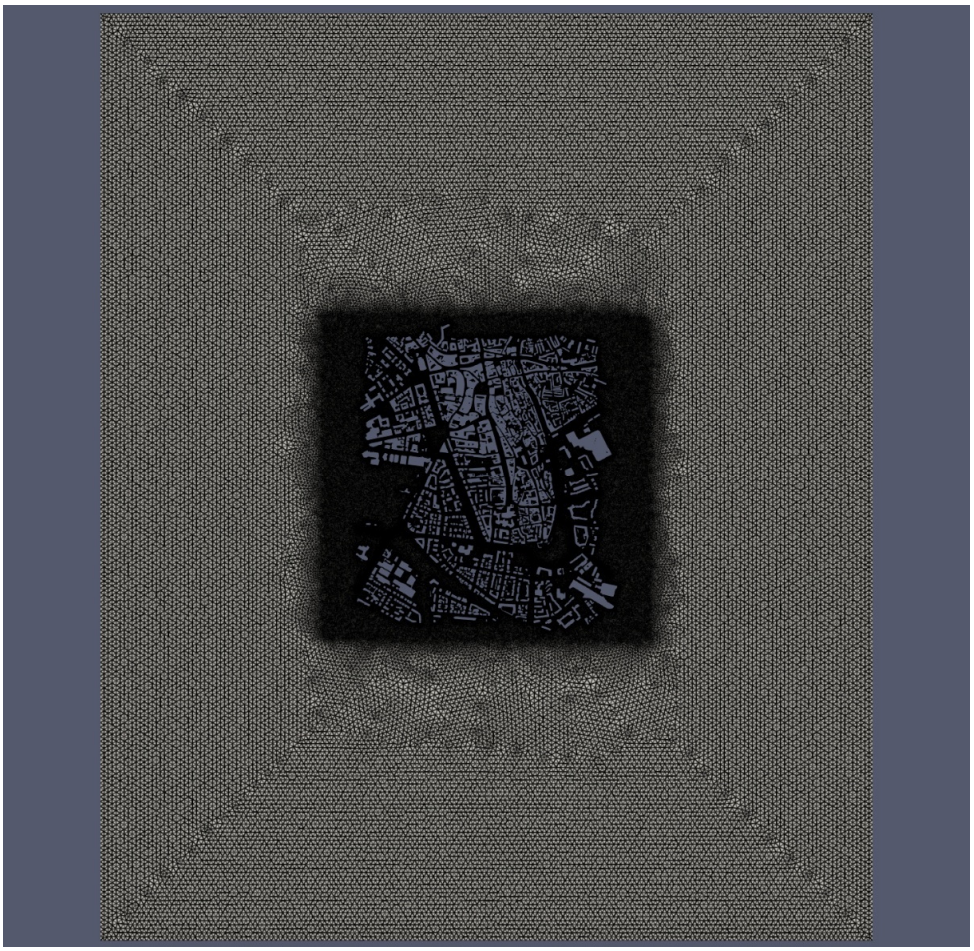

(**a**)

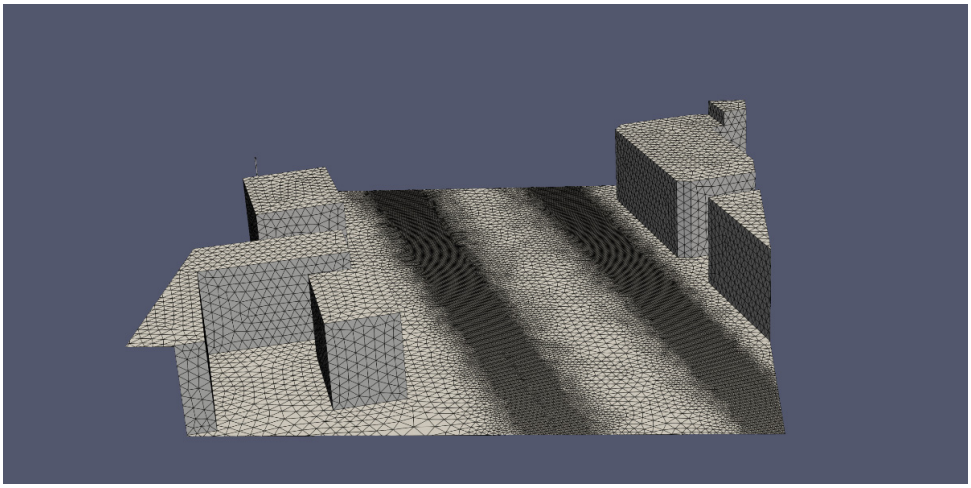

(**b**)

Figure 3. Computational mesh in the overall area and higher-density region in the $x - y$ plane (**a**) and on the ground, building surfaces, and traffic sources (**b**).

It should be noted that this computational grid has been used in previous studies involving different CFD modelling applications in the Augsburg case study [11,24,53], providing well-validated results. A more detailed description of the grid is given in Ioannidis et al. [24], which was the study that constructed both the 3D geometry model and the mesh.

To calculate pollutant concentrations within the spatial domain, emissions from 69 road traffic sources were used. The emission sources were selected on both major arterial roads and smaller but highly active streets. This combination of traffic sources was previously selected, utilized, and validated in the study by Ioannidis et al. [24] to comprehensively represent the traffic emission activity within the area of interest. A network of 81 measurement sensors was set up as the observational network for the current application. The heights of the sensor locations range from 2 to 4 m. In Figure 4, the traffic emission sources are illustrated in red lines, while the sensors are depicted in yellow dots in the $x - y$ plane.

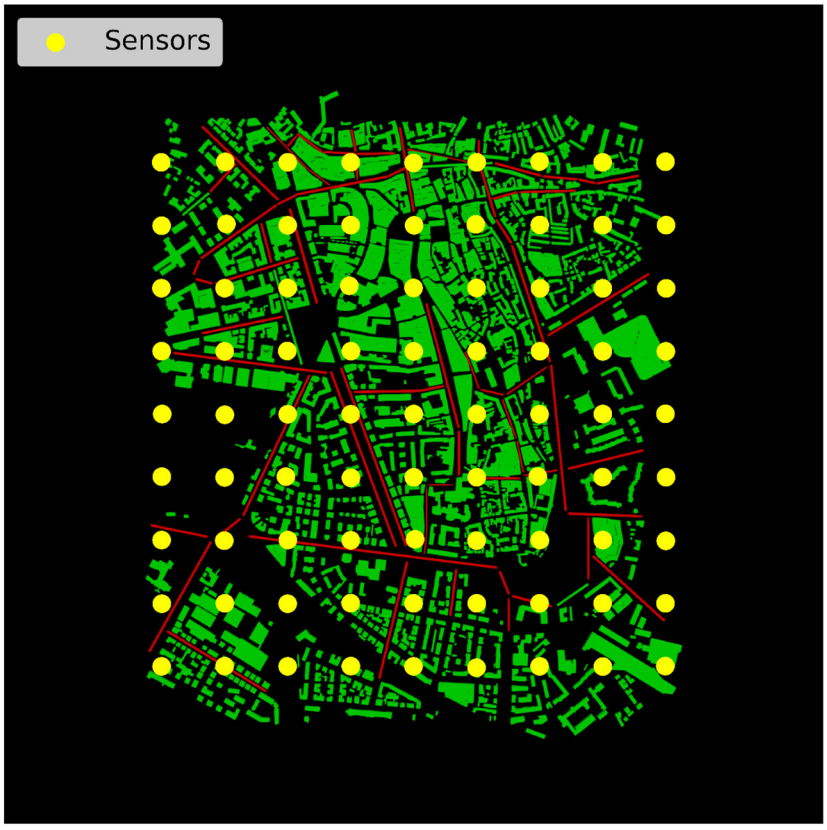

Figure 4. The locations the traffic emission sources illustrated in red lines and the positions of the sensors depicted in yellow dots in the $x - y$ plane.

2.5. Settings

2.5.1. Numerical Simulations Set up

For the numerical CFD simulations, the RANS approach is combined with the two-equation turbulence model $k - \varepsilon$ via the SIMPLE (simpleFoam) solver in the OpenFOAM v2112 CFD suite [57]. The solver was modified to resolve the forward advection-diffusion equation (Equation (3)) for each traffic source, meaning that 69 equations were introduced into the solver. In total, 36 numerical simulations were performed for a number of iterations long enough to achieve convergence in steady state.

Regarding the meteorological conditions, the assumptions of negligible thermal heat flux effects and neutral stability Atmospheric Boundary Layer (ABL) conditions were

adopted. This assumption aligns with the main CFD modelling for pollutant dispersion guidelines, such as those from the Association of German Engineers (Verein Deutscher Ingenieure—VDI) and the COST 732 group [58–60], and has been adopted in previous CFD pollutant dispersion implementations in real environments, providing accurate results [52,61,62]. For neutral stability conditions, the boundary conditions at the inlet can be specified following the equations of Richards and Hoxey [63]. The inflow velocity profile, $U(z)$, was calculated from Equation (13), where u^* is the friction velocity (Equation (14)), $\kappa = 0.41$ is the von Karman constant, and $z_0 = 2$ m is the aerodynamic roughness length. The reference velocity, U_{ref}, was set to 1 m/s at the reference height, z_{ref}, of 3 m. Therefore, in each wind direction, the inlet velocity was calculated from as follows:

$$U(z) = \frac{u^*}{\kappa} ln\left(\frac{z + z_0}{z_0}\right) \tag{13}$$

$$u^* = \frac{U_{ref}\kappa}{ln\left(\frac{z_{ref}+z_0}{z_0}\right)} \tag{14}$$

The turbulent kinetic energy, k, and the turbulence dissipation rate, ε, at the inlet boundaries were calculated from Equation (15) and Equation (16), respectively [63]:

$$k = \frac{(u^*)^2}{\sqrt{C_\mu}} \tag{15}$$

$$\varepsilon(z) = \frac{(u^*)^3}{\kappa(z + z_0)} \tag{16}$$

where $C_\mu = 0.09$ is a model constant.

Regarding the dispersion model boundary conditions, a uniform release rate of 1 kg/m^3 was set for each traffic source boundary and the Schmidt number was set to 0.7.

2.5.2. Metropolis–Hastings MCMC Set up

In each applied scenario, the Metropolis–Hastings MCMC algorithm was used to estimate the samples of the PDFs of the target variables, which in this application are the emission rates of the 69 road segments treated as individual traffic sources. Therefore, in the current work a total of 69 PDFs were calculated by the algorithm. Initialization involves a random estimate for each source release rate within a specific upper and lower bound. The assumption that each release rate proposal value should be within these bounds was followed in every iteration of the algorithm, since that assumption is the prior information of the current Bayesian process, as described in Section 2.3.2.

To determine the measurement and model bias ($\sigma_{o,i}^2 + \sigma_{c,i}^2$ in Equation (3) the approach from previous applications was followed, where t $\sigma_{o,i}^2 + \sigma_{c,i}^2 = a \times C^o{}_i$ [25,42]. Here, a is a constant specified by the user and is consistent across all sensors. In the present study, the constant a was set to 0.5. The total number of iterations for each run of the Metropolis–Hastings MCMC algorithm was 80,000, with a burn-in period of 20,000 iterations. The subsequent 60,000 samples were used for the collection of PDF samples.

2.6. Synthetic Observational Dataset

To address the absence of measurements from a dense monitoring network of a regulated air pollutant that is highly emitted by traffic activity, a synthetic observation dataset of a theoretical pollutant was generated by utilizing the forward dispersion model's concentrations and adding Gaussian noise to them. For each individual plume from the 69 sources, noise was added to the concentrations at the 81 sensor positions for every wind direction scenario. For the sensor configuration analysis, four wind direction scenarios were

selected to represent various wind conditions. Specifically, the chosen scenarios were 50, 140, 230, and 320 degrees. In each scenario, the synthetic observation dataset was generated such that the measured concentrations provide a $FAC2 = 0.5$ and $FAC4 = 1$, in comparison to the corresponding modelled concentrations. This ensures that representative noise was added for air pollution CFD modelling applications, with no extreme discrepancies between the modelled and observed concentrations.

3. Results

As described in previous section, the forward advection–diffusion equation was solved independently for each individual traffic source. Although this technique significantly increases the computational cost of the simulation compared to the traditional forward model, where pollutant dispersion was calculated within the same concentration field, it is necessary to store the source–receptor relationship fields. Since the source–receptor relationship describes the sensitivity of each source to every sensor position, this approach is crucial for understanding the contribution of each source to sensor observations. To illustrate this, pollutant concentration fields for some individual sources are presented. Figure 5a–d depicts four individual sources within the computational domain that were selected to visualize the independent plumes.

Figure 6a–d illustrates the corresponding concentration fields of the four sources for the 50-degree wind direction case in the $x - y$ plane at a height of 3 m. In all plume visualizations, the sensors of the measurement network are depicted as green dots, making the influence of each source on the various sensors apparent. Concentration fields are shown on a logarithmic scale, ranging from 10^{-8} kg/m^3 to 1 kg/m^3. Note that the corresponding plumes for the other investigated wind direction scenarios (140, 230, and 320 degrees) are presented in Appendix A.

Having presented some individual pollutant plumes, it is useful to visualize the overall concentration field as calculated from the forward dispersion model. Figure 7 shows the concentration field in the $x - y$ plane at a height of 1 m, combining contributions from all 69 sources and the corresponding measurement network (green dots) for the 50-degree wind direction case. The concentration field is displayed on a logarithmic scale ranging from 10^{-3} kg/m^3 to 1 kg/m^3. As indicated, the different sources (shown in Figure 6a–d) contribute differently to the overall pollutant concentrations. Similarly to the individual plumes, the overall concentration fields for the other three wind direction cases are also presented in Appendix A.

To evaluate the ability of the present methodology to provide accurate emission rate estimations and to investigate the impact of the number of sensors on these estimations, the Metropolis–Hastings MCMC algorithm was applied to different sensor configurations. The sensor configurations were divided into subgroups based on the number of sensors. The first subgroup consists of 10 sensors randomly selected from the total 81 sensors in each application of the algorithm. Each additional subgroup is formed by adding 10 more sensors until the total number is reached. Therefore, the created subgroups consist of 10, 20, . . ., up to 80 sensors.

To minimize the influence of potential random effects arising from the application parameters, which could result in either unusually high or lower quality solutions, the algorithm was applied to multiple sensor location combinations within each sensor group for every selected wind direction. Specifically, for each wind direction and sensor number subgroup, the algorithm was run 20 times using different randomly selected positions, resulting in a total of 80 PDF estimations for each of the 69 sources.

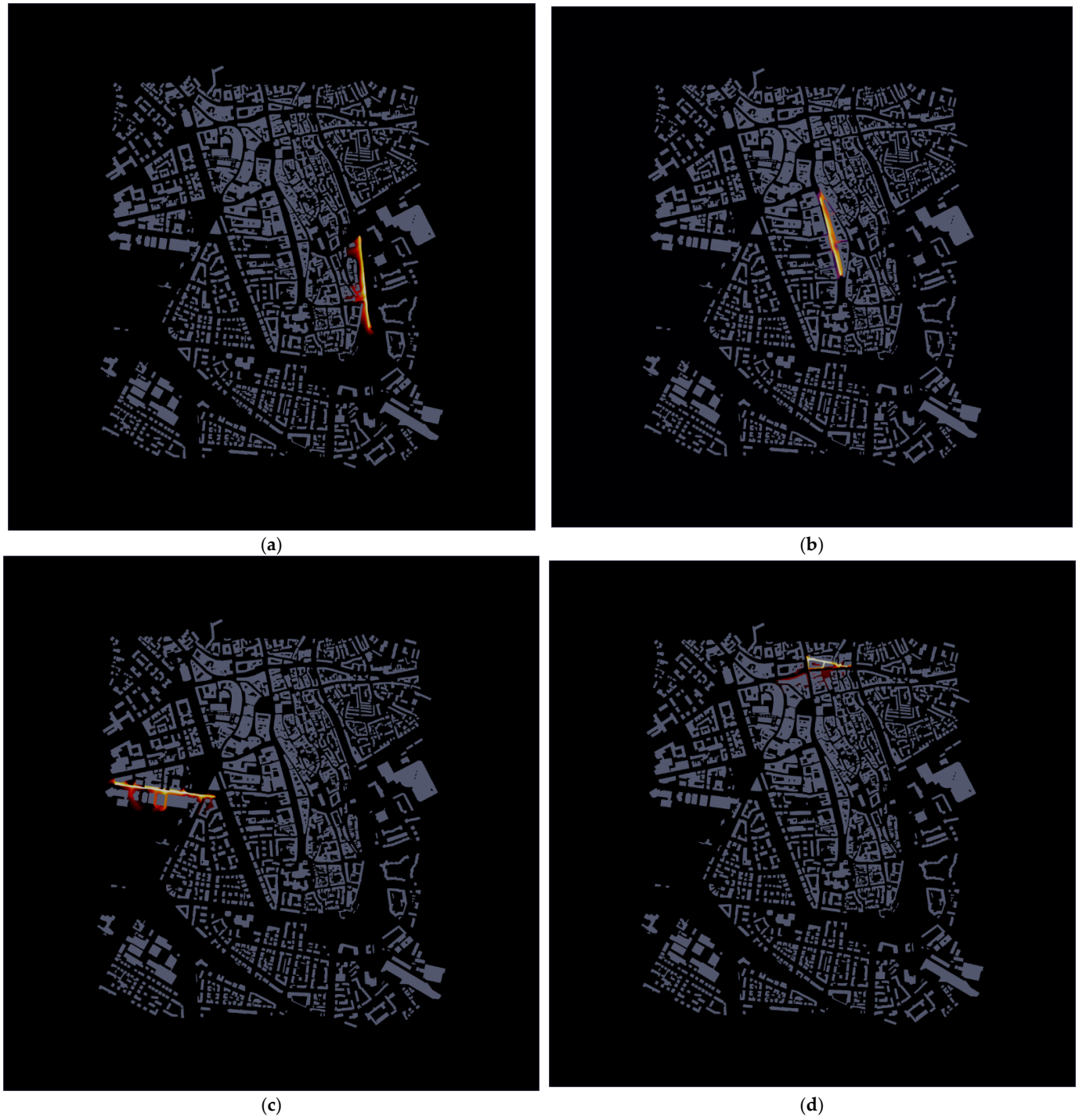

Figure 5. The four individual traffic emission sources (**a**–**d**) selected for the pollutant plume visualization.

To assess the quality of the calculated estimations, the release rate ratio Δq (Equation (17)) is determined based on the true and estimated release rates for each source. The target value for the release rate ratio Δq, it is unity ($\Delta q = 1$). It is important to note that the estimated release rate is defined as the mean value of the corresponding PDF.

$$\Delta q = max[(q_e/q_t), (q_t/q_e)] \tag{17}$$

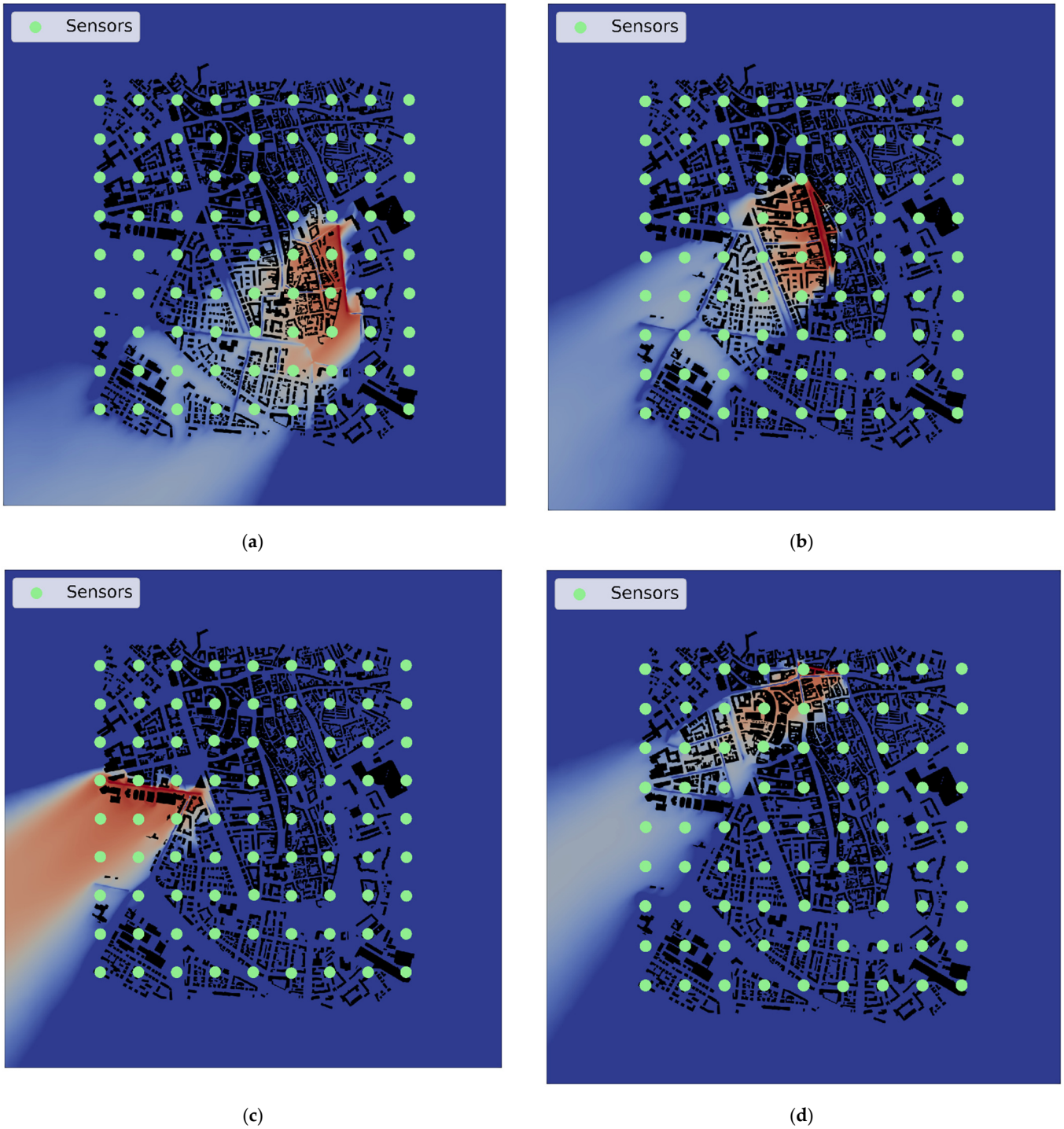

Figure 6. Pollutant plumes from four individual traffic emission sources (**a**–**d**) in $x - y$ plane at 3 m height for the 50 degrees wind direction scenario. The sensors are depicted with green dots.

Figures 8 and 9 present the findings of the analysis regarding how the number of sensors influences the estimation of release rates for multiple sources under different configurations and wind directions. Specifically, the boxplots depict the release rate ratios (Δq), calculated based on the mean values of the PDFs estimations for all 69 traffic sources across the 80 randomly selected configurations (20 configurations for each wind direction case) within each sensor number subgroup. It should be noted that the evaluation metric Δq is always greater than or equal to 1, with the ideal estimation being exactly 1. Figure 8 shows the results obtained using the Metropolis–Hastings MCMC algorithm with the

assumption that each emission rate falls within the range of 0.01 to 20 kg/s. In contrast, Figure 9 illustrates the results for a wider range, from 0.001 to 100 kg/s.

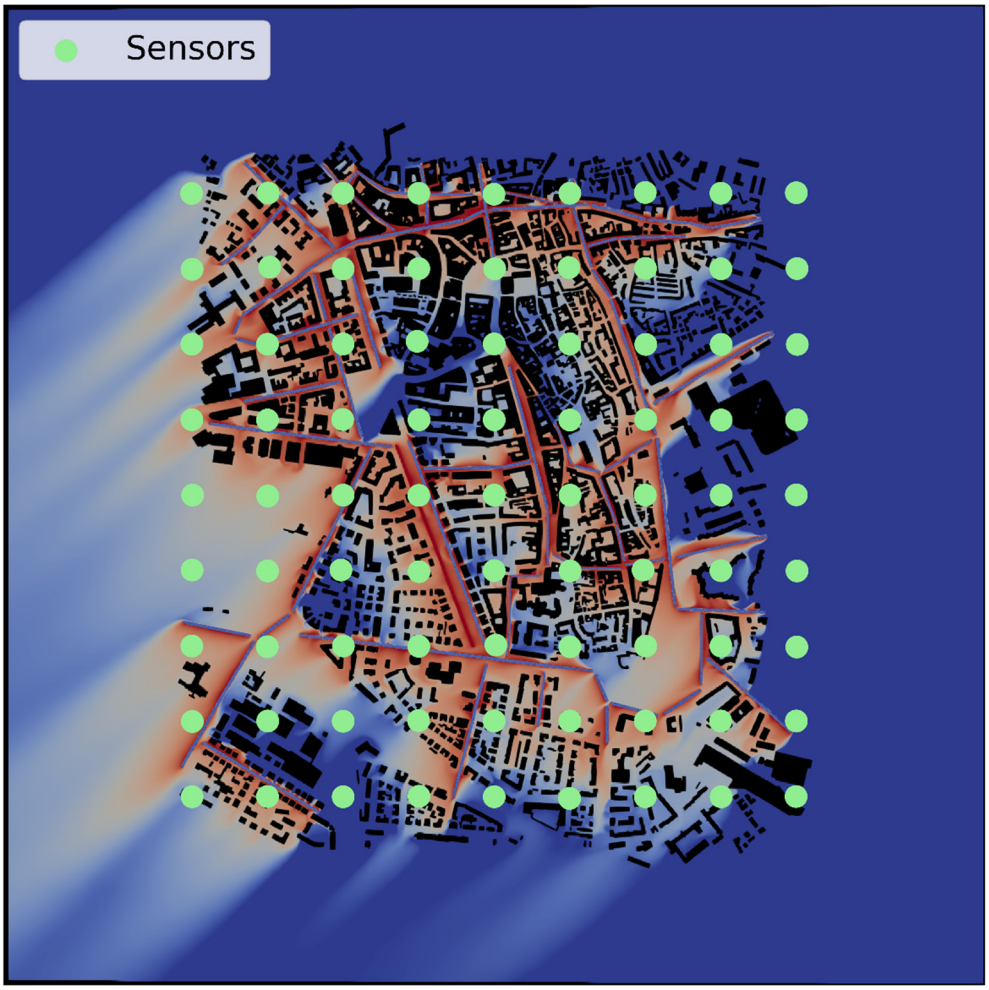

Figure 7. Overall pollutant concentration field from the 69 sources in $x - y$ plane at 3 m height for 50 degrees wind direction scenario. Sensors are shown with green dots.

As expected, the results in Figure 8 highlight that better solutions were generally achieved in subgroups utilizing a higher number of sensors. Specifically, for configurations with more than 60 sensors, the majority of the estimations have Δq values below 2, with many approaching 1.5, indicating very high-quality solutions, approaching the ideal value. Although the accuracy of most estimations decreases with a lower number of sensors, even in the subgroup with only 10 sensors, the algorithm provides satisfactory results, with most release rate ratios values been around 2.5. A notable observation is that increasing the number of sensors leads to wider boxplots. Furthermore, in the higher-number subgroups, some estimates exceed a Δq value of 3, unlike the lower-number subgroups. Overall, the fact that $\Delta q < 4$ is observed across all cases indicates a high level of accuracy for the entire application.

For a more comprehensive presentation of the results shown in Figures 8 and 9, Table 1 summarizes the statistics for each box in these figures.

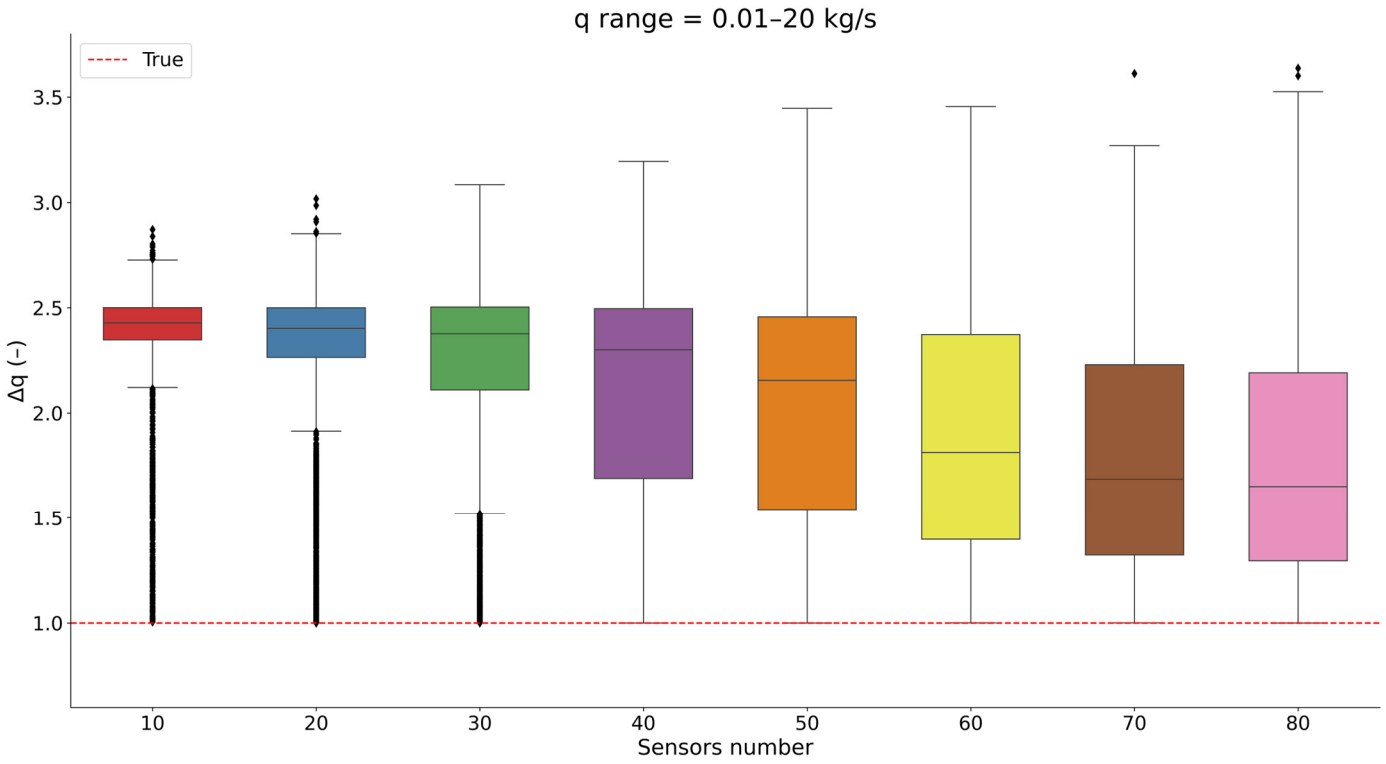

Figure 8. The release rate ratios Δq between the mean estimated and true source emission rates which range from 0.01 to 20 kg/s across all traffic sources in each sensor group. Each box illustrates the results of 80 random configurations, while the diamonds indicate the outlier values of the overall distribution. The red line represents the true values of the sources.

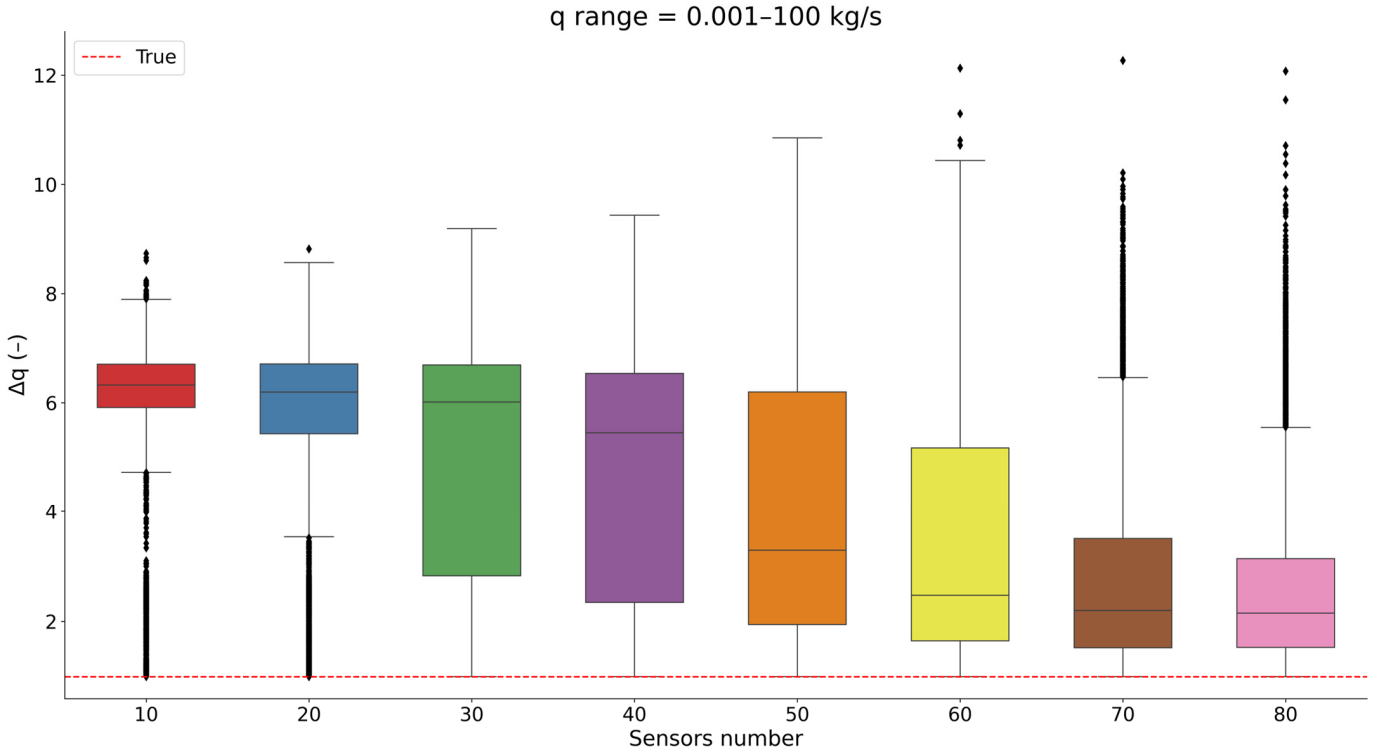

Figure 9. The release rate ratios Δq between the mean estimated and true source emission rates which range from 0.001 to 100 kg/s across all traffic sources in each sensor group. Each box illustrates the results of 80 random configurations, while the diamonds indicate the outlier values of the overall distribution. The red line represents the true values of the sources.

Table 1. Statistics of the distributions of estimated release rate ratios for each sensor subgroup under all applied scenarios.

Prior Knowledge	Sensor's Subgroup	Mean	Median	Std	Min	Max	Q 25%	Q 75%
q range = 0.001–100 kg/s	10	5.94	6.33	1.48	1.00	8.74	5.91	6.71
	20	5.51	6.20	1.88	1.00	8.82	5.43	6.71
	30	5.18	6.01	2.06	1.00	9.19	2.83	6.69
	40	4.64	5.45	2.25	1.00	9.44	2.34	6.54
	50	4.05	3.29	2.30	1.00	10.85	1.95	6.20
	60	3.38	2.47	2.17	1.00	12.13	1.65	5.17
	70	2.90	2.20	1.93	1.00	12.27	1.52	3.50
	80	2.76	2.15	1.79	1.00	12.07	1.53	3.14
q range = 0.01–20 kg/s	10	2.29	2.41	0.38	1.01	2.80	2.30	2.50
	20	2.21	2.37	0.44	1.01	2.86	2.19	2.49
	30	2.20	2.37	0.45	1.01	3.02	1.91	2.51
	40	2.06	2.24	0.50	1.00	3.05	1.62	2.46
	50	1.96	2.02	0.54	1.00	3.18	1.49	2.42
	60	1.84	1.74	0.52	1.00	3.46	1.41	2.30
	70	1.79	1.67	0.51	1.00	3.27	1.39	2.20
	80	1.77	1.66	0.51	1.00	3.42	1.38	2.18

The outcomes illustrated in Figure 9 highlight that increasing the uncertainty in the estimation of prior knowledge (by widening the permitted bounds for the release rates) leads to lower accuracy, especially in subgroups with fewer sensors. Although the boxplots of the subgroups show similar structures, significantly worse release rate estimations are observed in subgroups that use configurations with fewer than 60 sensors. Specifically, the lowest accuracy is observed in the 10 and 20 sensor subgroups, where the majority of Δq values lie around 6. On the other hand, higher quality solutions (with release rate ratios near the value of 2) are indicated in the 70 and 80 sensors subgroups, although a few estimates fail by providing a solution higher than an order of magnitude.

4. Discussion

In general, the findings of the application indicate that the novel methodology can provide accurate release rate estimates from multiple traffic sources in an urban environment by combining CFD numerical simulations with the Metropolis–Hastings MCMC algorithm. The only information used for the implementation is the data from the measurement network and some elementary prior knowledge about the range of each source's emission rate. As highlighted, reducing the range of prior information and increasing the number of sensors in the network leads to higher-quality solutions. The high performance of the application is demonstrated by the fact that the vast majority of the emission rate estimations were within an order of magnitude of the true release rates in both applied cases.

Moreover, when the potential range of release rates was relatively narrow (e.g., from 0.01 to 20 kg/s), all emission rate estimates yield a release rate ratio below 4. In the study by Kovalets et al. [64], a solution was considered of "good" quality when the release rate ratio Δq was less than 4. Therefore, in the present study, this criterion was satisfied for all sources when the allowable range of release rates was relatively small. When the bounds of the release rate range were expanded, there were numerous cases where the evaluation criterion was not met, particularly when fewer sensors were used. However, when the number of sensors exceeded 50, the vast majority of predictions result remained within a release rate ratio value $\Delta q < 4$.

The main limitation of this work is that the current methodology is evaluated solely on noisy synthetic observational datasets of a theoretical air pollutant, assuming the pollutant is a passive, non-reactive contaminant. Additionally, the methodology was tested on real measurement scenarios using observational data from the SmartAQnet [65] AQMN to estimate PM10 emissions from the 69 sources at an hourly temporal resolution. However, within the computational domain, real measurements were available from only five sensors. A broad prior range, spanning approximately seven orders of magnitude, was used for the release rate as prior knowledge of source emissions. However, the limited number of real sensors and the wide range of allowable emissions per source prevented the algorithm from converging to a solution.

To this end, further research is needed for AQ applications based on real measurements of a regulated pollutant correlated with traffic emissions. The absence of a dense, real-world AQMN within the area of interest makes it difficult to validate the present methodology under real-world conditions. Although the synthetic observational dataset was generated to represent real measurements ($FAC2 = 0.5$ and $FAC4 = 1$), and the algorithm was applied across multiple AQMN configurations and wind directions to reduce biases, the use of a synthetic pollutant without accounting for physical or chemical processes could still increase the uncertainties of the methodology. Moreover, since no previous studies have investigated emissions from multiple sources at street scale using CFD models, the results of this study cannot be directly compared with prior work. These factors highlight the importance of further implementing and evaluating the methodology against real observational datasets for regulated air pollutants, which is planned for future investigation.

Moreover, even though the 70 and 80 sensor networks, which indicated highly accurate solutions regardless of the prior knowledge of emission source rates, may seem like a very high number for a real measurement network in an urban environment, the increasing availability and accuracy of low-cost sensors, as well as the adoption of IoT policies within the framework of Smart Cities may lead to the design of such networks in the near future. Another interesting direction for further investigation is the utilization of several and more sophisticated Bayesian inference-based algorithms within the methodology, and comparison among their accuracy. Such work could provide useful insights about the exploration of the best fitted algorithm for such applications.

5. Conclusions

The main outcomes of the present study highlight that the proposed methodology is applicable for estimating emissions from multiple sources at street scale within real urban environments. The methodology can provide valuable information for identifying the primary air pollutant sources that contribute most to concentration levels and can be used to improve emission inventories. Additionally, it offers useful insights for the design of AQMNs in urban areas for inverse dispersion modelling applications. However, the limitations and assumptions adopted in this work indicate the need for further development, implementation, evaluation, and refinement of the methodology. To this end, the methodology is planned to be applied to regulated pollutants released from traffic sources and evaluated against real measurements. Furthermore, comparing the performance of several Bayesian-based algorithms could provide information useful for improving the accuracy of the methodology. Moreover, further investigation is needed to examine the accuracy of the methodology in relation to spatial characteristics and potential patterns that may lead to over- or underestimation of each source's release rate.

Author Contributions: Conceptualization, P.G. and N.M.; methodology, P.G., G.T. and N.M.; software, P.G., G.I. and P.T.; validation, P.G., E.C., G.T. and N.M.; formal analysis, P.G.; investigation, P.G., G.T. and N.M.; resources, C.V., T.R. and N.M.; data curation, P.G.; writing—original draft preparation, P.G.; writing—review and editing, P.G., G.T., G.I., P.T., T.R., E.C., C.V. and N.M.; visualization, P.G. and G.I.; supervision, N.M.; project administration, N.M.; funding acquisition, N.M. All authors have read and agreed to the published version of the manuscript.

Funding: This work is part of the first author's doctoral dissertation research, which is funded by the Helmholtz Association of German Research Centres through a Graduate School of the Centre for Climate and Environment (GRACE) at the Karlsruhe Institute of Technology (KIT) scholarship under funding number 51. Furthermore, this work is a part of the programme Helmholtz European Partnership for Technological Advancement (HEPTA).

Institutional Review Board Statement: Not applicable.

Informed Consent Statement: Not applicable.

Data Availability Statement: Dataset available on request from the authors.

Acknowledgments: The authors acknowledge support by the state of Baden-Württemberg through bwHPC. OPENFOAM® is a registered trademark of OpenCFD Limited, producer and distributor of the OpenFOAM software v2112 via www.openfoam.com (accessed on 19 August 2025).

Conflicts of Interest: The authors declare no conflicts of interest.

Appendix A

This Appendix contains illustrations of the pollutant plumes for four individual road traffic sources (Figure 6), as well as for the overall number of sources (Figure 7) for inflow directions of 140, 230, and 320 degrees.

The individual sources plumes are shown in Figure A1a–d (for 140 degrees), Figure A2a–d (for 230 degrees), and Figure A3a–d (for 320 degrees).

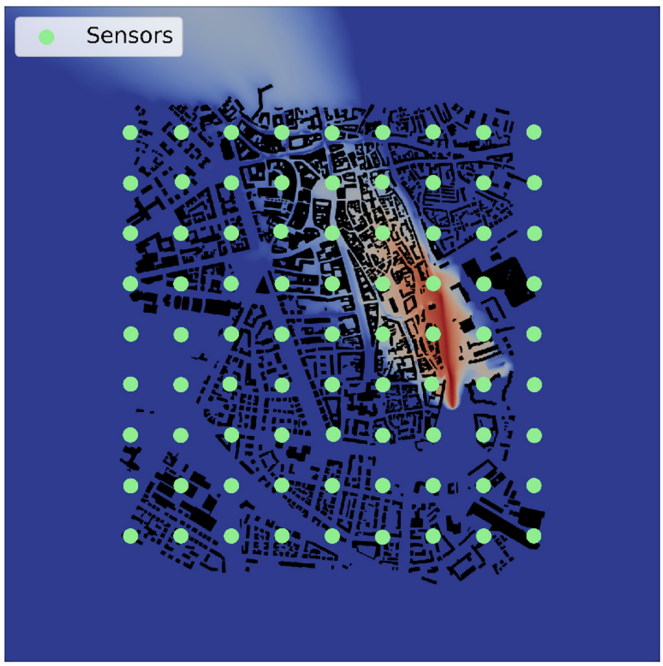

(**a**)

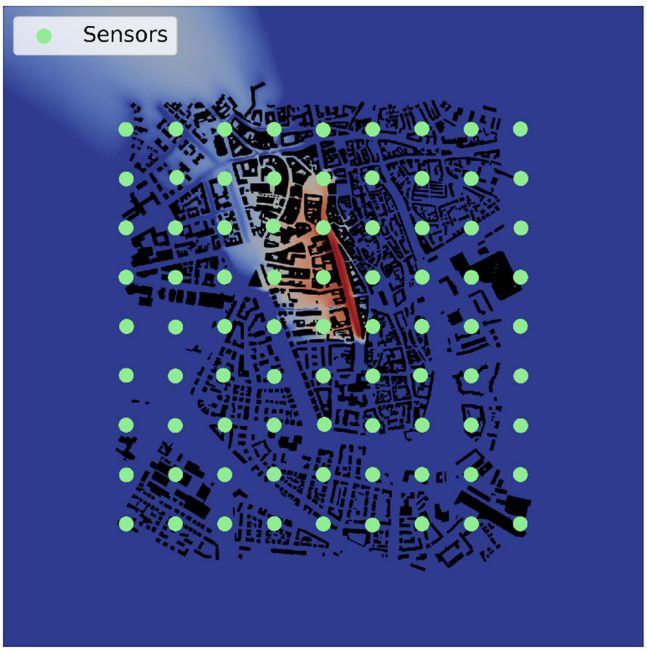

(**b**)

Figure A1. *Cont.*

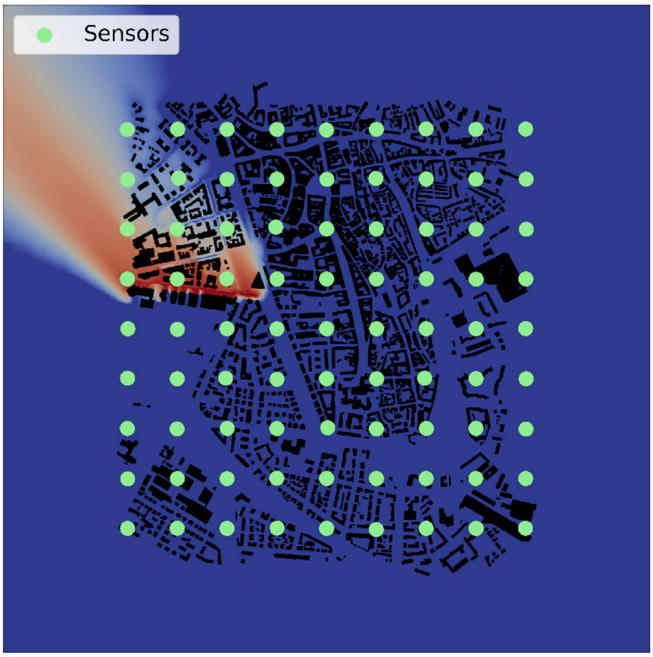

(**c**)

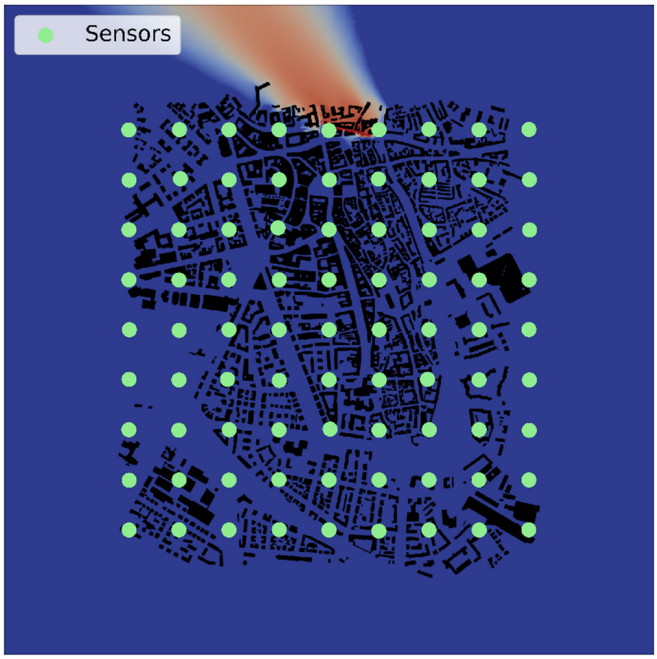

(**d**)

Figure A1. Pollutant plumes from four individual traffic emission sources (**a**–**d**) in $x - y$ plane at 3 m height for the 140 degrees wind direction scenario. The sensors are depicted with green dots.

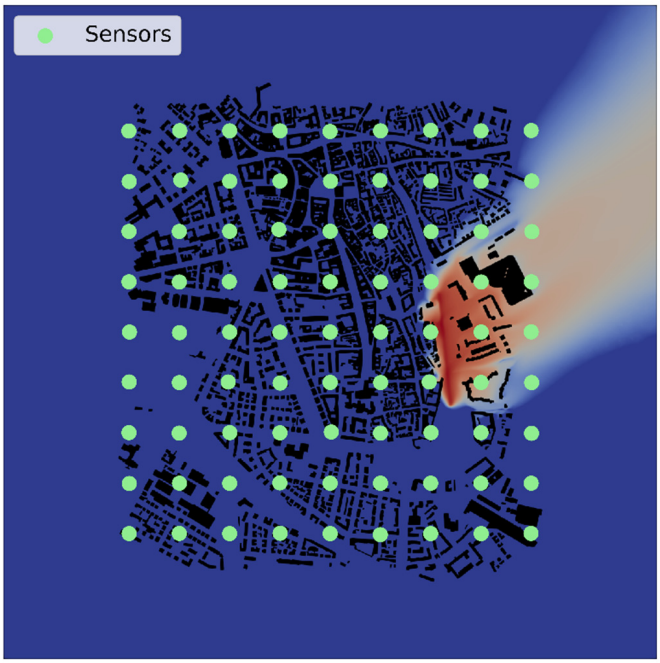

(**a**)

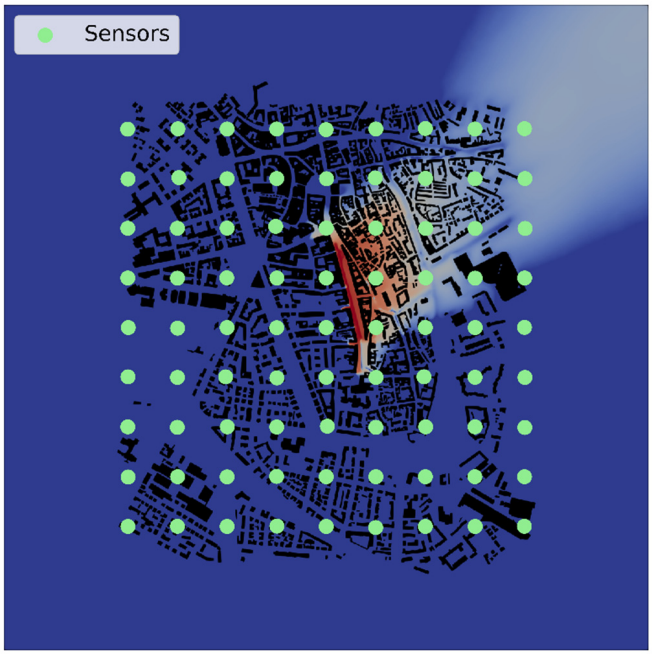

(**b**)

Figure A2. *Cont.*

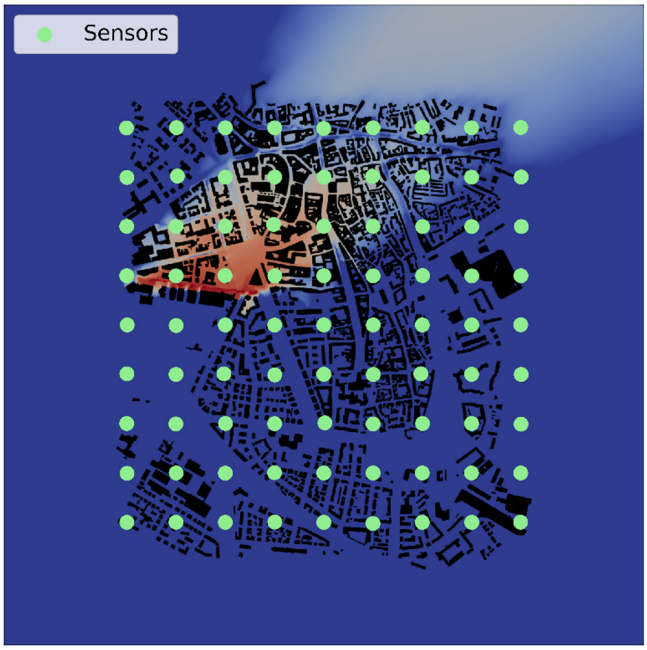

(**c**)

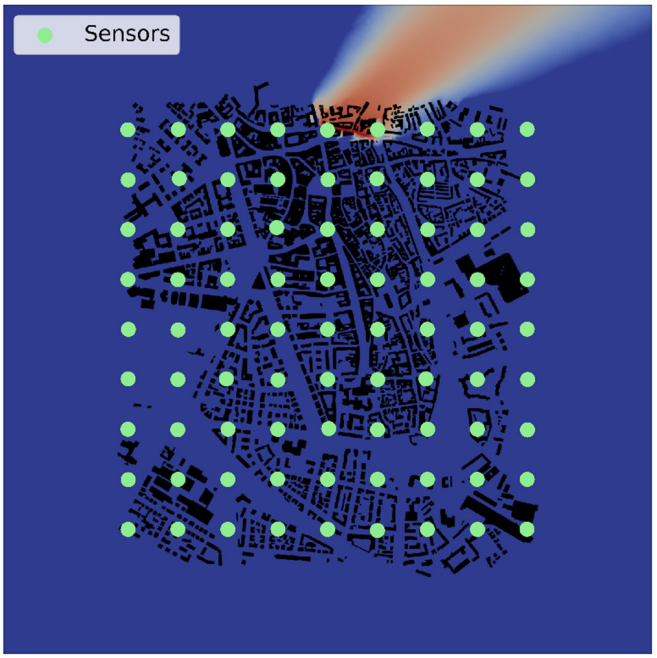

(**d**)

Figure A2. Pollutant plumes from four individual traffic emission sources (**a**–**d**) in $x - y$ plane at 3 m height for the 230 degrees wind direction scenario. The sensors are depicted with green dots.

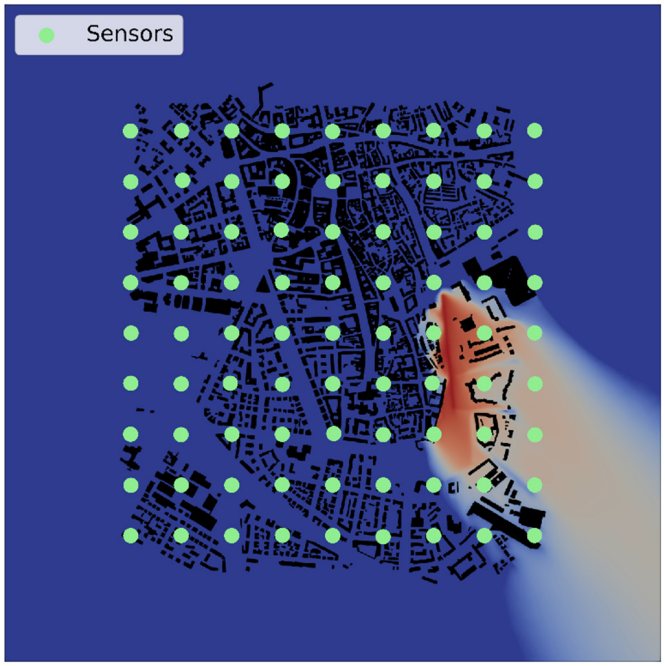

(**a**)

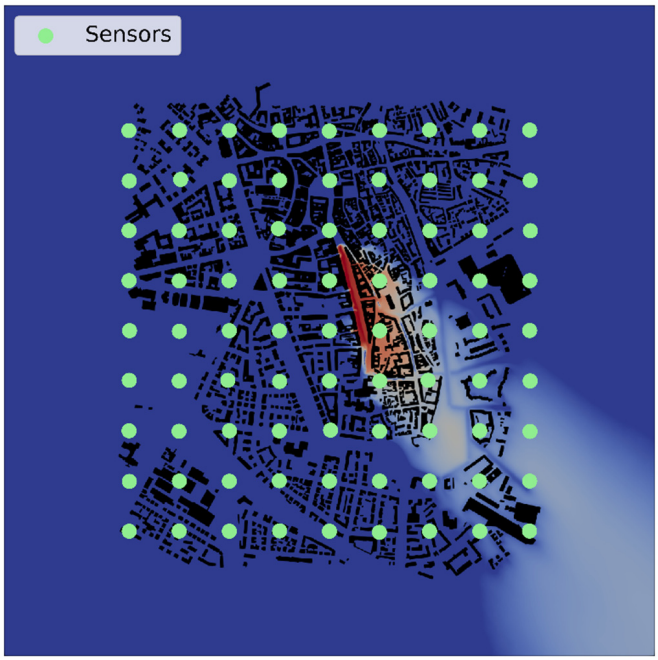

(**b**)

Figure A3. *Cont.*

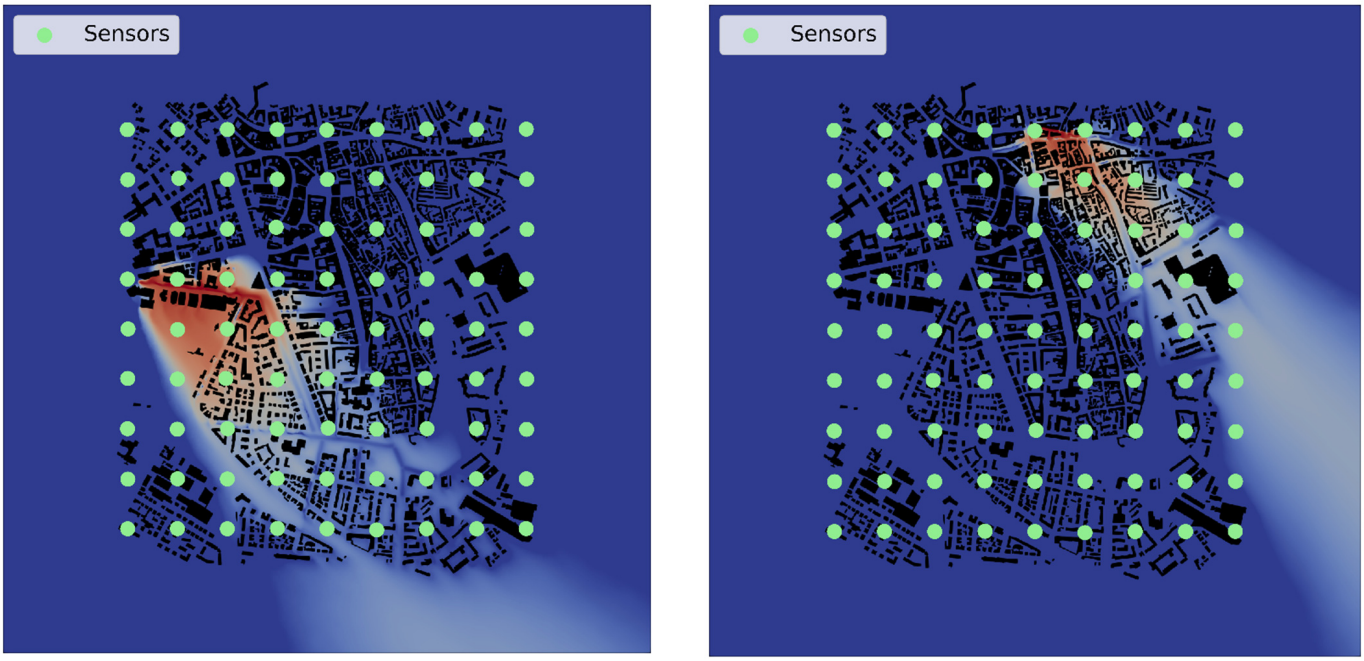

(**c**) (**d**)

Figure A3. Pollutant plumes from four individual traffic emission sources (**a**–**d**) in $x - y$ plane at 3 m height for the 320 degrees wind direction scenario. The sensors are depicted with green dots.

Figures A4–A6 present the pollutant concentrations plumes from all sources for the wind direction of 140 (Figure A4), 230 (Figure A5), and 320 (Figure A6) degrees.

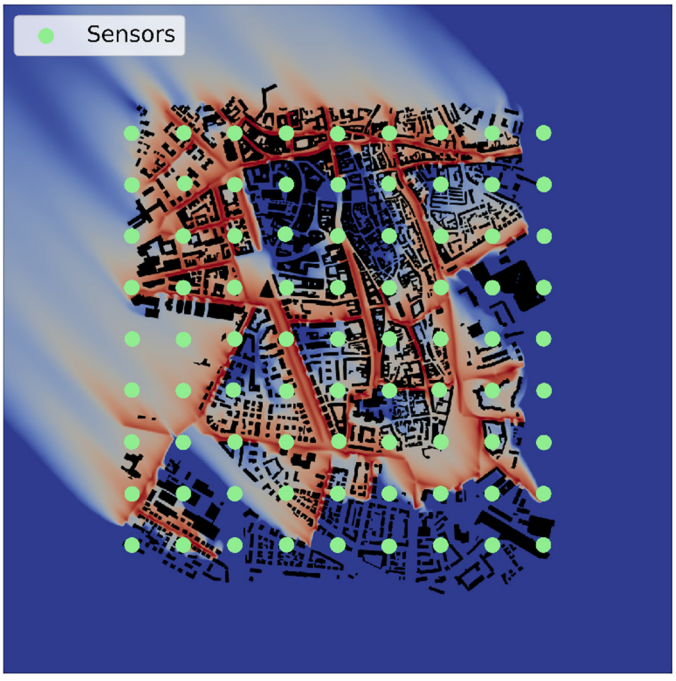

Figure A4. Overall pollutant concentration field from the 69 sources in $x - y$ plane at 3 m height for the 140 degrees wind direction scenario. The sensors are shown with green dots.

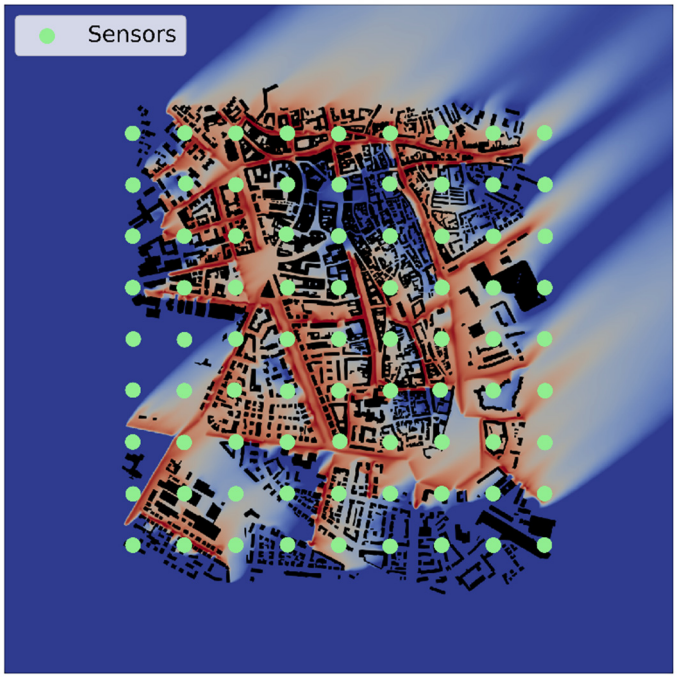

Figure A5. Overall pollutant concentration field from the 69 sources in $x - y$ plane at 3 m height for the 230 degrees wind direction scenario. The sensors are shown with green dots.

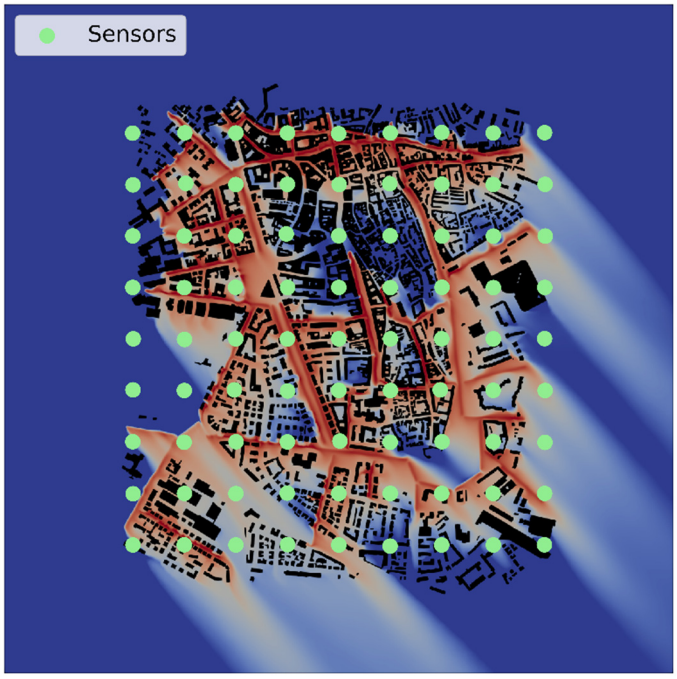

Figure A6. Overall pollutant concentration field from the 69 sources in $x - y$ plane at 3 m height for the 320 degrees wind direction scenario. The sensors are shown with green dots.

References

1. Moussiopoulos, N. *Air Quality in Cities*; Springer Science & Business Media: Berlin/Heidelberg, Germany, 2003.
2. Vlachokostas, C.; Banias, G.; Athanasiadis, A.; Achillas, C.; Akylas, V.; Moussiopoulos, N. Cense: A Tool to Assess Combined Exposure to Environmental Health Stressors in Urban Areas. *Environ. Int.* **2014**, *63*, 1–10.
3. World Health Organization; others WHO Global. *Air Quality Guidelines: Particulate Matter (PM2. 5 and PM10), Ozone, Nitrogen Dioxide, Sulfur Dioxide and Carbon Monoxide*; World Health Organization: Geneva, Switzerland, 2021.

4. Hutchinson, M.; Oh, H.; Chen, W.H. A Review of Source Term Estimation Methods for Atmospheric Dispersion Events Using Static or Mobile Sensors. *Inf. Fusion* **2017**, *36*, 130–148. [CrossRef]
5. Pudykiewicz, J.A. Application of Adjoint Tracer Transport Equations for Evaluating Source Parameters. *Atmos. Environ.* **1998**, *32*, 3039–3050. [CrossRef]
6. Kobayashi, T.; Nagai, H.; Chino, M.; Kawamura, H. Source Term Estimation of Atmospheric Release Due to the Fukushima Dai-Ichi Nuclear Power Plant Accident by Atmospheric and Oceanic Dispersion Simulations: Fukushima NPP Accident Related. *J. Nucl. Sci. Technol.* **2013**, *50*, 255–264. [CrossRef]
7. Terada, H.; Katata, G.; Chino, M.; Nagai, H. Atmospheric Discharge and Dispersion of Radionuclides during the Fukushima Dai-Ichi Nuclear Power Plant Accident. Part II: Verification of the Source Term and Analysis of Regional-Scale Atmospheric Dispersion. *J. Environ. Radioact.* **2012**, *112*, 141–154. [CrossRef]
8. Kopka, P.; Wawrzynczak, A. Framework for Stochastic Identification of Atmospheric Contamination Source in an Urban Area. *Atmos. Environ.* **2018**, *195*, 63–77. [CrossRef]
9. Gkirmpas, P.; Barmpas, F.; Tsegas, G.; Moussiopoulos, N.; Vlachokostas, C. Unknown Source Parameters Estimation in an Urban-Like Domain Using RANS and LES Approaches. In *Air Pollution Modeling and Its Application XXIX*; Mensink, C., Mathur, R., Arunachalam, S., Eds.; Springer Nature Switzerland: Cham, Switzerland, 2025; pp. 181–187.
10. Yee, E.; Hoffman, I.; Ungar, K. Bayesian Inference for Source Reconstruction: A Real-World Application. *Int. Sch. Res. Not.* **2014**, *2014*, 507634. [CrossRef]
11. Gkirmpas, P.; Tsegas, G.; Ioannidis, G.; Vlachokostas, C.; Moussiopoulos, N. Identification of an Unknown Stationary Emission Source in Urban Geometry Using Bayesian Inference. *Atmos. Atmos.* **2024**, *15*, 871. [CrossRef]
12. Singh, S.K.; Rani, R. A Least-Squares Inversion Technique for Identification of a Point Release: Application to Fusion Field Trials 2007. *Atmos Environ.* **2014**, *92*, 104–117. [CrossRef]
13. Singh, S.K.; Turbelin, G.; Issartel, J.-P.; Kumar, P.; Feiz, A.A. Reconstruction of an Atmospheric Tracer Source in Fusion Field Trials: Analyzing Resolution Features. *J. Geophys. Res. Atmos.* **2015**, *120*, 6192–6206. [CrossRef]
14. Yee, E. Probability Theory as Logic: Data Assimilation for Multiple Source Reconstruction. *Pure Appl. Geophys.* **2012**, *169*, 499–517. [CrossRef]
15. Zhang, H.L.; Li, B.; Shang, J.; Wang, W.W.; Zhao, F.Y. Source Term Estimation for Continuous Plume Dispersion in Fusion Field Trial-07: Bayesian Inference Probability Adjoint Inverse Method. *Sci. Total Environ.* **2024**, *915*, 169802. [CrossRef]
16. Efthimiou, G.C.; Kovalets, I.V.; Venetsanos, A.; Andronopoulos, S.; Argyropoulos, C.D.; Kakosimos, K. An Optimized Inverse Modelling Method for Determining the Location and Strength of a Point Source Releasing Airborne Material in Urban Environment. *Atmos. Environ.* **2017**, *170*, 118–129. [CrossRef]
17. Efthimiou, G.C.; Kovalets, I.V.; Argyropoulos, C.D.; Venetsanos, A.; Andronopoulos, S.; Kakosimos, K.E. Evaluation of an Inverse Modelling Methodology for the Prediction of a Stationary Point Pollutant Source in Complex Urban Environments. *Build. Environ.* **2018**, *143*, 107–119. [CrossRef]
18. Gkirmpas, P.; Barmpas, F.; Tsegas, G.; Efthimiou, G.; Tremper, P.; Riedel, T.; Vlachokostas, C.; Moussiopoulos, N. An Evaluation of the Sensitivity of a Source Term Estimation Methodology of Sensor Configuration in an Urban-like Environment. *Atmosphere* **2024**, *15*, 1512. [CrossRef]
19. Allen, C.T.; Young, G.S.; Haupt, S.E. Improving Pollutant Source Characterization by Better Estimating Wind Direction with a Genetic Algorithm. *Atmos. Environ.* **2007**, *41*, 2283–2289. [CrossRef]
20. Allen, C.T.; Haupt, S.E.; Young, G.S. Source Characterization with a Genetic Algorithm–Coupled Dispersion–Backward Model Incorporating SCIPUFF. *J. Appl. Meteorol. Clim.* **2007**, *46*, 273–287. [CrossRef]
21. Haupt, S.E.; Young, G.S.; Allen, C.T. Validation of a Receptor–Dispersion Model Coupled with a Genetic Algorithm Using Synthetic Data. *J. Appl. Meteorol. Clim.* **2006**, *45*, 476–490. [CrossRef]
22. Santiago, J.L.; Borge, R.; Martin, F.; de la Paz, D.; Martilli, A.; Lumbreras, J.; Sanchez, B. Evaluation of a CFD-Based Approach to Estimate Pollutant Distribution within a Real Urban Canopy by Means of Passive Samplers. *Sci. Total Environ.* **2017**, *576*, 46–58. [CrossRef]
23. Sanchez, B.; Santiago, J.L.; Martilli, A.; Martin, F.; Borge, R.; Quaassdorff, C.; de la Paz, D. Modelling NOX Concentrations through CFD-RANS in an Urban Hot-Spot Using High Resolution Traffic Emissions and Meteorology from a Mesoscale Model. *Atmos. Environ.* **2017**, *163*, 155–165. [CrossRef]
24. Ioannidis, G.; Tremper, P.; Li, C.; Riedel, T.; Rapkos, N.; Boikos, C.; Ntziachristos, L. Integrating Cost-Effective Measurements and CFD Modeling for Accurate Air Quality Assessment. *Atmosphere* **2024**, *15*, 1056. [CrossRef]
25. Keats, A.; Yee, E.; Lien, F.-S. Bayesian Inference for Source Determination with Applications to a Complex Urban Environment. *Atmos. Environ.* **2007**, *41*, 465–479. [CrossRef]
26. Haupt, S.E. A Demonstration of Coupled Receptor/Dispersion Modeling with a Genetic Algorithm. *Atmos. Environ.* **2005**, *39*, 7181–7189. [CrossRef]

27. Lu, J.; Huang, M.; Wu, W.; Wei, Y.; Liu, C. Application and Improvement of the Particle Swarm Optimization Algorithm in Source-Term Estimations for Hazardous Release. *Atmosphere* **2023**, *14*, 1168. [CrossRef]
28. Wawrzynczak, A.; Kopka, P.; Borysiewicz, M. Sequential Monte Carlo in Bayesian Assessment of Contaminant Source Localization Based on the Sensors Concentration Measurements. In Proceedings of the Parallel Processing and Applied Mathematics: 10th International Conference, PPAM 2013, Warsaw, Poland, 8–11 September 2013; Revised Selected Papers, Part II 10. 2014; pp. 407–417.
29. Ickowicz, A.; Septier, F.; Armand, P.; Delignon, Y. Adaptive Bayesian Algorithms For The Estimation Of Source Term In A Complex Atmospheric Release. In Proceedings of the 15th International Conference on Harmonisation within Atmospheric Dispersion Modelling for Regulatory Purposes, Madrid, Spain, 6–9 May 2013.
30. Wang, R.; Chen, B.; Qiu, S.; Ma, L.; Zhu, Z.; Wang, Y.; Qiu, X. Hazardous Source Estimation Using an Artificial Neural Network, Particle Swarm Optimization and a Simulated Annealing Algorithm. *Atmosphere* **2018**, *9*, 119. [CrossRef]
31. Ling, Y.; Yue, Q.; Chai, C.; Shan, Q.; Hei, D.; Jia, W. Nuclear Accident Source Term Estimation Using Kernel Principal Component Analysis, Particle Swarm Optimization, and Backpropagation Neural Networks. *Ann. Nucl. Energy* **2020**, *136*, 107031. [CrossRef]
32. Coelho, S.; Ferreira, J.; Rodrigues, V.; Lopes, M. Source Apportionment of Air Pollution in European Urban Areas: Lessons from the ClairCity Project. *J. Environ. Manag.* **2022**, *320*, 115899. [CrossRef]
33. Feng, X.; Zhang, X.; Wang, J. Update of SO_2 Emission Inventory in the Megacity of Chongqing, China by Inverse Modeling. *Atmos. Environ.* **2023**, *294*, 119519.
34. Cheng, X.; Hao, Z.; Zang, Z.; Liu, Z.; Xu, X.; Wang, S.; Liu, Y.; Hu, Y.; Ma, X. A New Inverse Modeling Approach for Emission Sources Based on the DDM-3D and 3DVAR Techniques: An Application to Air Quality Forecasts in the Beijing–Tianjin–Hebei Region. *Atmos. Chem. Phys.* **2021**, *21*, 13747–13761.
35. Kumar, S.; Sharma, S.; Sharma, P.; Agarwal, S. Inverse Modelling Approach to Assess Air Pollutant Emission Trends, and Source Contributions in Highly Polluted Cities. *Discov. Atmos.* **2024**, *2*, 13.
36. Ntziachristos, L.; Gkatzoflias, D.; Kouridis, C.; Samaras, Z. COPERT: A European Road Transport Emission Inventory Model. In Proceedings of the Information Technologies in Environmental Engineering: Proceedings of the 4th International ICSC Symposium, Thessaloniki, Greece, 28–29 May 2009; pp. 491–504.
37. Carruthers, D.; Stidworthy, A.; Clarke, D.; Dicks, J.; Jones, R.; Leslie, I.; Popoola, O.A.M.; Seaton, M. Urban Emission Inventory Optimisation Using Sensor Data, an Urban Air Quality Model and Inversion Techniques. *Int. J. Environ. Pollut.* **2019**, *66*, 252–266. [CrossRef]
38. Xue, F.; Li, X.; Ooka, R.; Kikumoto, H.; Zhang, W. Turbulent Schmidt Number for Source Term Estimation Using Bayesian Inference. *Build. Environ.* **2017**, *125*, 414–422. [CrossRef]
39. Xue, F.; Kikumoto, H.; Li, X.; Ooka, R. Bayesian Source Term Estimation of Atmospheric Releases in Urban Areas Using LES Approach. *J. Hazard. Mater.* **2018**, *349*, 68–78. [CrossRef]
40. Henry, F.; Bonifacio, R.G.M.; Glasgow, L.A. Numerical Simulation of Transport of Particles Emitted From Ground-Level Area Source Using Aermod and CFD. *Eng. Appl. Comput. Fluid. Mech.* **2014**, *8*, 488–502. [CrossRef]
41. Wang, Y.; Huang, H.; Huang, L.; Ristic, B. Evaluation of Bayesian Source Estimation Methods with Prairie Grass Observations and Gaussian Plume Model: A Comparison of Likelihood Functions and Distance Measures. *Atmos. Environ.* **2017**, *152*, 519–530. [CrossRef]
42. Jia, H.; Kikumoto, H. Source Term Estimation in Complex Urban Environments Based on Bayesian Inference and Unsteady Adjoint Equations Simulated via Large Eddy Simulation. *Build. Environ.* **2021**, *193*, 107669. [CrossRef]
43. Metropolis, N.; Rosenbluth, A.W.; Rosenbluth, M.N.; Teller, A.H.; Teller, E. Equation of State Calculations by Fast Computing Machines. *J. Chem. Phys.* **1953**, *21*, 1087–1092. [CrossRef]
44. Kahn, H.; Marshall, A.W. Methods of Reducing Sample Size in Monte Carlo Computations. *J. Oper. Res. Soc. Am.* **1953**, *1*, 263–278. [CrossRef]
45. Von Neumann, J. Various Techniques Used in Connection with Random Digits. *John Von. Neumann Collect. Work.* **1963**, *5*, 768–770.
46. Gordon, N.J.; Salmond, D.J.; Smith, A.F.M. Novel Approach to Nonlinear/Non-Gaussian Bayesian State Estimation. In *IEE Proceedings F (Radar and Signal Processing)*; IET: London, UK, 1993; Volume 140, pp. 107–113.
47. Gilks, W.R.; Richardson, S.; Spiegelhalter, D. *Markov Chain Monte Carlo in Practice*, 1st ed.; Chapman and Hall/CRC: New York, NY, USA, 1995. [CrossRef]
48. Haklay, M.; Weber, P. Openstreetmap: User-Generated Street Maps. *IEEE Pervasive Comput.* **2008**, *7*, 12–18. [CrossRef]
49. Haklay, M. How Good Is Volunteered Geographical Information? A Comparative Study of OpenStreetMap and Ordnance Survey Datasets. *Environ. Plan. B Plan. Des.* **2010**, *37*, 682–703. [CrossRef]
50. Mooney, P.; Corcoran, P.; Winstanley, A.C. Towards Quality Metrics for OpenStreetMap. In Proceedings of the 18th SIGSPATIAL International Conference on Advances in Geographic Information Systems, San Jose, CA, USA, 2–5 November 2010; pp. 514–517.
51. Neis, P.; Zielstra, D.; Zipf, A. The Street Network Evolution of Crowdsourced Maps: OpenStreetMap in Germany 2007–2011. *Future Internet* **2011**, *4*, 1–21. [CrossRef]

52. Ioannidis, G.; Li, C.; Tremper, P.; Riedel, T.; Ntziachristos, L. Application of CFD Modelling for Pollutant Dispersion at an Urban Traffic Hotspot. *Atmosphere* **2024**, *15*, 113. [CrossRef]
53. Antoniou, A.; Ioannidis, G.; Ntziachristos, L. Realistic Simulation of Air Pollution in an Urban Area to Promote Environmental Policies. *Environ. Model. Softw.* **2024**, *172*, 105918. [CrossRef]
54. Blocken, B. Computational Fluid Dynamics for Urban Physics: Importance, Scales, Possibilities, Limitations and Ten Tips and Tricks towards Accurate and Reliable Simulations. *Build. Environ.* **2015**, *91*, 219–245. [CrossRef]
55. *BETA CAE Systems ANSA Pre-Processor Software*, Version 20.1.0 2020; BETA CAE Systems: Thessaloniki, Greece, 2019.
56. Ariff, M.; Salim, S.M.; Cheah, S.C. *Wall Y+ Approach for Dealing with Turbulent Flows over a Surface Mounted Cube: Part 2—High Reynolds Number*; CSIRO Publishing: Melbourne, Australia, 2009.
57. OpenFOAM Foundation Ltd. OpenFOAM V2112: The Open Source CFD Toolbox 2021. OpenFOAM Foundation Ltd.: London, UK, 2021.
58. VDI. *VDI 3783 Part 9: Environmental Meteorology. Prognostic Microscale Wind Field Models. Evaluation for Flow around Buildings and Obstacles*; VDI/DIN-Kommission Reinhaltung der Luft (KRdL)-Normenausschuss: Düsseldorf, Germany, 2017.
59. VDI. *VDI 3783 Part 4: Environmental Meteorology—Acute Accidental Releases into the Atmosphere—Requirements to an Optimal System to Determining and Assessing Pollution of the Atmosphere*; VDI/DIN-Kommission Reinhaltung der Luft (KRdL)-Normenausschuss: Düsseldorf, Germany, 2004.
60. Franke, J.; Hellsten, A.; Schlünzen, H.; Carissimo, B. *COST–Best Practice Guideline for the CFD Simulation of Flows in the Urban Environment*; University of Hamburg: Hamburg, Germany, 2007.
61. Martín, F.; Janssen, S.; Rodrigues, V.; Sousa, J.; Santiago, J.L.; Rivas, E.; Stocker, J.; Jackson, R.; Russo, F.; Villani, M.G.; et al. Using Dispersion Models at Microscale to Assess Long-Term Air Pollution in Urban Hot Spots: A FAIRMODE Joint Intercomparison Exercise for a Case Study in Antwerp. *Sci. Total Environ.* **2024**, *925*, 171761. [CrossRef]
62. Rivas, E.; Santiago, J.L.; Lechón, Y.; Martín, F.; Ariño, A.; Pons, J.J.; Santamaría, J.M. CFD Modelling of Air Quality in Pamplona City (Spain): Assessment, Stations Spatial Representativeness and Health Impacts Valuation. *Sci. Total Environ.* **2019**, *649*, 1362–1380. [CrossRef]
63. Richards, P.J.; Hoxey, R.P. Appropriate Boundary Conditions for Computational Wind Engineering Models Using the K-ε Turbulence Model. *Comput. Wind Eng.* **1993**, *46*, 145–153. [CrossRef]
64. Kovalets, I.V.; Andronopoulos, S.; Venetsanos, A.G.; Bartzis, J.G. Identification of Strength and Location of Stationary Point Source of Atmospheric Pollutant in Urban Conditions Using Computational Fluid Dynamics Model. *Math. Comput. Simul.* **2011**, *82*, 244–257. [CrossRef]
65. Budde, M.; Riedel, T.; Beigl, M.; Schäfer, K.; Emeis, S.; Cyrys, J.; Schnelle-Kreis, J.; Philipp, A.; Ziegler, V.; Grimm, H.; et al. SmartAQnet: Remote and in-Situ Sensing of Urban Air Quality. In Proceedings of the Remote Sensing of Clouds and the Atmosphere XXII, Warsaw, Poland, 11–14 September 2017; Volume 10424, pp. 19–26.